Geophysical Journal International

Geophys. J. Int. (2018) **213,** 1768–1784
Advance Access publication 2018 February 23
GJI heat flow and volcanology

doi: 10.1093/gji/ggy073

Influence of conduit flow mechanics on magma rheology and the growth style of lava domes

Taha Husain,[1] Derek Elsworth,[1] Barry Voight,[2] Glen Mattioli[3] and Pamela Jansma[3]

[1]*Energy and Mineral Engineering, G3 Center and EMS Energy Institute, The Pennsylvania State University, University Park, PA* 16802*, USA.*
E-mail: taha.husain@shell.com
[2]*Geosciences, The Pennsylvania State University, University Park, PA* 16802*, USA*
[3]*Department of Earth and Environmental Sciences, University of Texas at Arlington, Arlington, TX* 76019*, USA*

Accepted 2018 February 22. Received 2018 February 16; in original form 2017 June 12

SUMMARY

We develop a 2-D particle-mechanics model to explore different lava-dome growth styles. These range from endogenous lava dome growth comprising expansion of a ductile dome core to the exogenous extrusion of a degassed lava plug resulting in generation of a lava spine. We couple conduit flow dynamics with surface growth of the evolving lava dome, fuelled by an open-system magma chamber undergoing continuous replenishment. The conduit flow model accounts for the variation in rheology of ascending magma that results from degassing-induced crystallization. A period of reduced effusive flow rates promote enhanced degassing-induced crystallization. A degassed lava plug extrudes exogenously for magmas with crystal contents (ϕ) of 78 per cent, yield strength >1.62 MPa, and at flow rates of <0.5 m^3 s^{-1}, while endogenous dome growth is predicted at higher flow rates ($Q_{\text{out}} > 3$ m^3 s^{-1}) for magma with lower relative yield strengths (<1 MPa). At moderately high flow rates ($Q_{\text{out}} = 4$ m^3 s^{-1}), the extrusion of magma with lower crystal content (62 per cent) and low interparticulate yield strength (0.6 MPa) results in the development of endogenous shear lobes. Our simulations model the periodic extrusion history at Mount St. Helens (1980–1983). Endogenous growth initiates in the simulated lava dome with the extrusion of low yield strength magma ($\phi = 0.63$ and $\tau_p = 0.76$ MPa) after the crystallized viscous plug ($\phi = 0.87$ and $\tau_p = 3$ MPa) at the conduit exit is forced out by the high discharge rate pulse ($2 < Q_{\text{out}} < 12$ m^3 s^{-1}). The size of the endogenous viscous plug and the occurrence of exogenous growth depend on magma yield strength and the magma chamber volume, which control the periodicity of the effusion. Our simulations generate dome morphologies similar to those observed at Mount St Helens, and demonstrate the degree to which domes can sag and spread during and following extrusion pulses. This process, which has been observed at Mount St. Helens and other locations, largely reflects gravitational loading of dome with a viscous core, with retardation by yield strength and talus friction.

Key words: Numerical modelling; Planetary volcanism; Eruption mechanisms and flow emplacement; Lava rheology and morphology.

1 INTRODUCTION

Fluctuation in extrusion rates at Soufriere Hills Volcano (SHV), Montserrat and at Mount St. Helens (MSH), USA is semi-periodic, with periods of high discharge rate alternating with periods of low extrusion rate (Melnik & Sparks 2005). The fluctuation in extrusion rate influences the rate of volatile exsolution, which subsequently controls degassing-induced crystallization that is promoted by decompression during magma ascent (Sparks *et al.* 2000).This results in rheological stiffening due to an increase in the total magma crystal content and gas-loss from melt (Lejeune & Richet 1995; Hess & Dingwell 1996; Sparks 1997; Hort 1998; Melnik & Sparks 1999; Cashman & Blundy 2000; Hammer & Rutherford 2002; Costa 2005; Cashman *et al.* 2008). The extent of rheological stiffening, controlled by the gain in mechanical strength, influences the observed flow patterns in the lava dome (Lavallée *et al.* 2007). Magma emplacement at SHV transitions between crystalline material with higher strength extruded as spines at low ascent rates (~0.5 to 2 m^3 s^{-1}) to that of endogenous growth of a viscous Newtonian fluid at higher flow rates (between 2 and 8 m^3 s^{-1}) (Sparks *et al.* 2000; Watts *et al.* 2002; Hale & Wadge 2008).

Observations of dome growth provide an invaluable source of information to define the evolution of magma rheology during

emplacement (Murase *et al*. 1985; Anderson & Fink 1990; Swanson & Holcomb 1990). Extrusion of Newtonian magma generates relatively low, smooth-surfaced domes (Huppert *et al.* 1982; Buisson & Merle 2002). Domes formed by highly crystalline magma with yield strength exhibit shear lobes and spine growth, which indicates the significance of internal yield strength on behaviour (Blake 1990; Griffiths & Fink 1997; Griffiths 2000; Hale *et al*. 2007; Hale 2008; Hale & Wadge 2008). Numerical models of a crystal rich magma can represent the observed transition in flow regime from endogenous to exogenous growth (Hale 2008; Husain *et al.* 2014). However a remaining question is whether such transitions are linked to deeper parts of the magma system. Conduit flow models have been capable of monitoring inputs of magma to the chamber and the subsequent discharge of volatile and crystal rich magma from a conduit, but thus far have not been linked to the surface morphology of an evolving lava dome (Melnik & Sparks, 1999, 2002, 2005; Barmin *et al.* 2002; Huppert & Woods 2002).

Other useful observations concern cyclic extrusion behaviour, which occurs at some volcanoes on a wide range of timescales (subdaily to multidecadal), accompanied by cycles of repetitive ground deformation, degassing and explosions (Voight *et al.* 1998, 1999; Young *et al*. 2003; Odbert *et al.* 2014). Here we consider subdaily to subannual cycles of activity, that can reflect the magma chamber, conduit, and dome-feedback conditions, which can influence lava dome morphology.

In this paper we evaluate the variation in magma rheology and dome morphology for the range of extrusion rates observed at SHV, Montserrat and MSH, USA (Sparks *et al.* 1998; Barmin *et al.* 2002; Mastin 2002; Watts *et al.* 2002; Cashman *et al.* 2008; Wadge *et al.* 2010). Rheological stiffening during ascent changes magma from Newtonian fluid to a crystalline solid and results in the transition in flow behaviour from an endogenously evolving dome to the exogenous extrusion of lava (Husain *et al.* 2014). Here our objective is to represent the effect of extrusion rate on magma rheology and explain the mechanism behind the observed evolution of lava dome morphology during cycles of magma extrusion. We use a 2-D discrete element modelling technique (Cundall & Strack 1979), as developed in our previous work (Husain *et al.* 2014), where a synthetic lava dome grows by extrusion from below a horizontal plane. In this case we couple our particle-mechanics model with a conduit flow model to investigate the effect of different magma plumbing conditions on the dynamics of the emplacement and the morphology of the lava dome. We consider the effect of crystal growth rate on enhancement of strength of the extruding magma and internal flow within a synthetic lava dome, and investigate the effect of fluctuating discharge rate on dome morphology. Parameters from analogue models of conduit flow inferred from the observations of periodic magma extrusion at MSH (1980–1986) (Barmin *et al.* 2002).

In the subsequent section (Section 3), we describe the development of the model with its relevant concepts in detail and list the model assumptions. Section 4 discusses model results, with the first part (section 4.1) considering the different intra-dome flow patterns with varying extrusion rate and magma yield strength, with parameters inferred from experimental studies and numerical conduit models for SHV (Couch *et al.* 2003; Melnik & Sparks 2005). Section 4.2 then develops a model to investigate the variation in lava dome morphology during periodic magma extrusion, with input parameters inferred from data at MSH during a period of cyclic extrusion (1980–1983) (Swanson & Holcomb 1990; Barmin *et al.* 2002).

2 MODEL CONCEPTS

Volcanic eruptions involve complex interacting processes, which are necessarily governed by nonlinear equations and many variables. Available modelling strategies vary between complex numerical models that incorporate many parameters, to simple models, which attempt capture the critical physical features of the process with simplifying assumptions (Barmin *et al.* 2002). Here we simplify analysis using the assumption that the conduit is separated into two zones, containing low and high viscosity fluids. The magma chamber is assumed surrounded by elastic wall rock and experiences periodic cycles of pressurization and de-pressurization due to the replenishment of magma from a deeper source and at a constant rate (Elsworth *et al.* 2008; Foroozan *et al.* 2010). The pressurization promotes magma ascent and related decompression that in turn causes the exsolution of volatile sand results in degassing-induced crystallization (Cashman & Blundy 2000; Sparks *et al.* 2000). An increase in total crystal content results in a rheological transition at depth x_T (distance from the magma chamber) from a lower initial magma viscosity (μ_1) to the higher viscosity (μ_2) (Lejeune & Richet 1995). Fig. 1 represents this process schematically.

The rate of crystallization during magma ascent controls the rheological state of the magma in the conduit. Magma in the conduit can flow under either of two different regimes: (1) rapid ascent of lower viscosity magma, which inhibits crystal growth and decreases transition depth, or (2) slower ascent which aids volatile loss and enhances crystal growth. The second case promotes crystallinity and results in rheological stiffening within the conduit. This approach (Barmin *et al.* 2002) is capable of simulating cycles of periodic discharge of magma that vary in amplitude and frequency, and which are governed by the input parameters assigned.

The growth of a lava dome initiates at the point of extrusion of high-viscosity magma at the conduit vent. The dome growth style (endogenous or exogenous) during the evolution of a synthetic lava dome is largely a function of the yield strength of the extruding magma, which in turn is governed by the magma crystal volume fraction (Voight *et al.* 1999; Saar *et al.* 2001; Watts *et al.* 2002). An increase in crystal content ultimately results in the formation of a continuous crystal phase in the magma, accompanied by significant enhancement in magma yield strength. At the critical volume fraction ϕ_c (dependent on crystal shape and size distributions) a continuous crystal network first forms to provide some minimum yield strength ($\tau_p \rightarrow 0$). For $\phi > \phi_c$, yield strength rapidly increases with increasing ϕ. The fluid-to-solid transition occurs at the maximum crystal packing fraction, ϕ_m, a value also dependent on crystal shape and size distributions (Saar *et al.* 2001). Note that this 'maximum' volume fraction defines the packing crystal content only at the fluid-solid transition, and that crystallization can continue within the pores of the packing structure. Thus the total crystal volume fraction in a volcanic rock can approach 100 per cent.

The model we present here couples conduit flow processes with the mechanics of lava dome flow emplacement. The model asserts simplifying assumptions for flow mechanics and phase behaviour, while providing information on the rheological behaviour of an evolving lava dome driven by a magma chamber experiencing periodic cycles of pressurization.

3 MODEL DEVELOPMENT

We develop a 2-D particle-mechanics model capable of mapping stress distribution and the evolution of flow morphology in a deforming aggregate. The magma is represented as an aggregate of

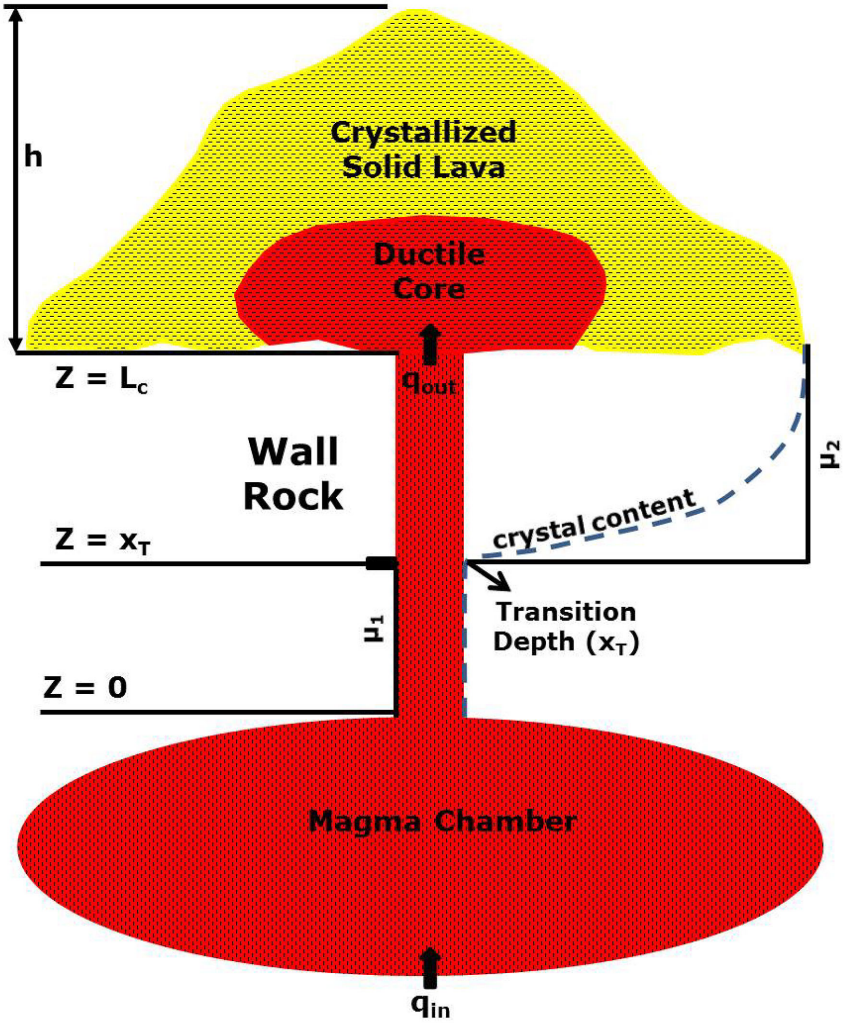

Figure 1. Diagrammatic representation of the conceptual model for the volcanic system during a lava dome building eruption. The chamber (ellipsoidal) surrounded by wall rock is pressurized by constant injection of magma (q_{in}) leads to discharge of magma (q_{out}) at the surface ($Z = L_c$). The ascending magma rheologically stiffens due to degassing-induced crystallization from an initial viscosity (μ_1) to a higher viscosity (μ_2) at a specific depth (x_T). The eruption of the highly crystalline magma results in the evolution of a lava dome of certain height (h) with a ductile core and a solid outer shell that can break up to form lava blocks and talus.

discrete particles (3 m diameter (D) in this study; Cundall & Strack 1979) where elastic deformation uses soft particle dynamics, which govern particle-particle interactions (Morgan & McGovern 2005a, Morgan & McGovern 2005a,b; Husain *et al.* 2014). In our model, a synthetic 2-D lava dome grows on a rigid horizontal base fed by a vertical conduit with a specified flow velocity. The width of the central vent in the 2-D model is specified as equal to the presumed radius of the conduit at SHV, Montserrat for section 4.1 and equal to the conduit radius of MSH, USA for section 4.2. Figs 2(a) and (c) represents the basic 2-D model in PFC^{2D} for the simulation runs with the dimensions given in Table 1.

The flow of high viscosity fluid through a conduit with a very small width to length ratio is assumed to be fully developed (Stasiuk & Jaupart 1997). Magma flow through the conduit during the eruptive cycle is in the laminar regime (Reynolds number of 5×10^{-11} in nature) for non-explosive eruptions (Jaupart & Tait 1990; Buisson & Merle 2002). The flow velocity of the magma (composed of a mixture of melt and crystals) in the conduit is calculated as shown by Barmin *et al.* (2002). Flow is controlled by a viscosity (μ) that is dependent on the volume concentration of crystals, represented as a step function. The system of equations to calculate flow velocity (u) for the unsteady case for a constant cross-sectional area is given as

$$\frac{\partial \rho}{\partial t} + \frac{\partial (\rho u)}{\partial z} = 0 \tag{1}$$

$$\frac{\partial n}{\partial t} + \frac{\partial (nu)}{\partial z} = 0 \tag{2}$$

$$\frac{\partial P}{\partial z} = -\rho g - \frac{8\mu u}{r_c{}^2};\ \mu = \begin{cases} \mu_1, \phi < \phi_T \\ \mu_2, \phi \geq \phi_T \end{cases} \tag{3}$$

$$\frac{\partial \phi}{\partial t} + u\frac{\partial \phi}{\partial z} = (36\pi n)^{1/3}\phi^{2/3}\chi, \tag{4}$$

where the magma density (ρ) in eq. (1) is considered constant during an increase in crystal content (ϕ) for instantaneous nucleation of crystals at a specified linear crystal growth rate (χ). The number density of crystals per unit volume (n) in eq. (2) in the conduit is fixed and is equal to that in the magma chamber (n_{ch}). The flow velocity is calculated (eq. 3) for a given gradient in vertical (z)

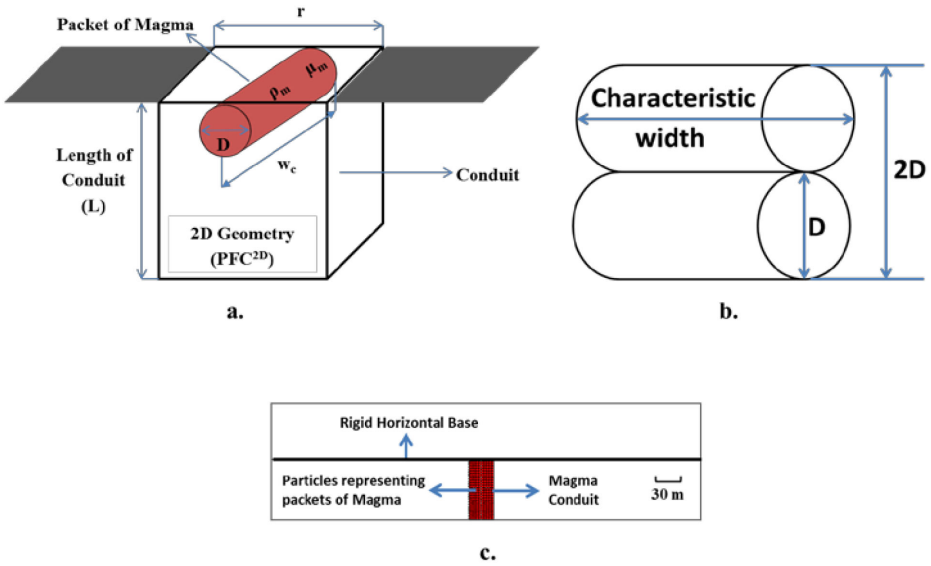

Figure 2. (a) Representation of PFC^{2D} model geometry in 3-D. (b) Shape of the particle used in the simulation run and area perpendicular to applied force. (c) Basic model setup in PFC^{2D} which includes the conduit (30 m wide opening for the simulation model in Section 4.1 and 18 m for Section 4.2) where the lava dome develops on a rigid horizontal surface (700 m long on either side of the conduit) and the red particles of 1.5 m radius represent magma that forms the volatile rich magma that forms the core in the lava dome.

Table 1. PFC model dimensions.

Conduit length (2-D)	Equivalent conduit radius (3-D)	Conduit width (2-D)	Depth of Conduit (2-D)	Expanse of the base
30 m	15 (9[a]) m	23.5725 m	300 m	1400 m

[a]Parameters for the simulation runs in Section 4.2 for Mount St. Helens.

pressure $\partial P/\partial z$ and for a specified conduit radius (r_c), where the viscosity changes from μ_1 to μ_2 for a volume concentration (ϕ) higher than the threshold transitional value (ϕ_T). The total crystal content (ϕ) at a given depth (z) is calculated (eq. 4) for a constant linear crystal growth rate (χ) (Marsh 1998; Cashman & Blundy 2000). The boundary conditions for flow through the conduit are given as,

$$z = 0 : \frac{\mathrm{d}P_{\mathrm{ch}}}{\mathrm{d}t} = \frac{\gamma}{V_{\mathrm{ch}}}\left[Q_{\mathrm{in}} - Q_{\mathrm{out}}\right]; \phi = \phi_{\mathrm{ch}}; n = n_{\mathrm{ch}} \tag{5}$$

$$z = L_c : P = \rho g h, \tag{6}$$

where the magma chamber pressure (P_{ch}) at time (t) for a specified chamber volume (V_{ch}) is a function of the net efflux (difference between the constant influx Q_{in} and total outflow Q_{out}) for a surrounding wallrock of given rigidity (γ). The volume concentration of crystals (ϕ_{ch}) and crystal density per unit volume (n_{ch}) of magma at the chamber are considered constant. The pressure at the conduit exit at a distance L_c from the magma chamber is a function of the lava dome height (h) (Fig. 1). The method to obtain the quasi-static solution for the system of equations (eqs 1–4) is given in Melnik & Sparks (2002) and the variation in flow rate with chamber pressure is obtained by solving for the boundary conditions given by eqs (5) and (6) (see Fig. 1 for a schematic representation). The calculated flow velocity is assigned as input to the discrete particles in the particle-mechanics model and in this manner, we simulate the effect of variable flow rate on the lava dome morphology, as reflected by the periodic pressurization of the magma chamber, and the volatile-loss triggering of rheological stiffening in the conduit.

Upon extrusion from the conduit exit, the particle-particle contact is assumed to develop bond strength. The evolution of the bond strength is governed by the volumetric crystal fraction of the magma, which is given as (Saar *et al.* 2001),

$$\tau_p = \tau_0 \left[\frac{\phi/(1-\phi_c)}{(1-\phi)/\phi_m}\right], \tag{7}$$

where τ_p and τ_0 are respectively, the non-Newtonian yield strength, and interparticulate resistance to hydrodynamic forces for a specified critical (ϕ_c) and maximum crystal content (ϕ_m). In the Saar *et al.* (2001) study the critical crystal volume fraction varied from 0.08 to 0.29, depending on crystal shape and randomness of orientation. The values of maximum packing fraction are less clear; Saar *et al.* (2001) cited the value 0.74, which is the maximum packing value for uniform spheres (e.g. Shaw 1965), but recognized that the value would differ for non-spherical crystals of different sizes. Marsh (1981) had suggested a value around 0.60. The maximum packing fraction for the Saar *et al.* (2001) model was calculated at 0.74.

At Montserrat, Watts *et al.* (2002) had suggested that solidification of spines or mega-spines was largely completed (90–95 per cent) in the upper conduit, prior to extrusion, with cooling playing a negligible role. Such values exceed the maximum packing that defines the transition from a fluid to a solid, implying that the material was well within the solid range at time of extrusion.

Magma yield strength derived from experiments, observational inferences, and simulation results vary over a wide range, and with the magma composition, and method employed (10^3–10^8 Pa; e.g. Blake 1990; Pinkerton & Stevenson 1992; Lyman *et al.* 2005; Simmons *et al.* 2005; Hale 2007). The yield strength calculated from

eq. (7) is applied to the parallel bond that controls the failure behaviour of the particle-particle contact.

An approximation used to describe the non-Newtonian behaviour of magma flow is the Bingham flow law where shear stress (τ) is given by

$$\tau = \tau_p + \eta \dot{\gamma}, \tag{8}$$

where τ_p is the yield strength and η is the plastic viscosity for a strain rate of $\dot{\gamma}$. Flow initiates upon the application of a stress greater than the yield strength (τ_p) as represented by eq. (8). The apparent viscosity (η_{app}) can be used to define flow of the bulk fluid and is given as (Blake 1990; Griffiths 2000)

$$\eta_{\text{app}} = \eta + \frac{\tau_p}{\dot{\gamma}}, \tag{9}$$

where apparent viscosities calculated for the dacite magma at MSH are observed to vary from 10^{12} to 10^{9} Pa s for strain rates between 10^{-10} and 10^{-2} s^{-1} (Pinkerton & Stevenson 1992). The total shear force (F_t^s) is associated with the parallel contact bond in PFC^{2D} at time t after time step Δt and is given by

$$F_t^s = F_{t-\Delta t}^s + \Delta F_{\Delta t}^s, \tag{10}$$

where $F_{\Delta t}^s$ is the incremental shear force generated over the timestep Δt. Upon the application of a shear force ($F_{t-\Delta t}^s$) that exceeds the maximum shear stress (τ_p) the parallel bond fails (eq. 10). The maximum shear stress (τ_p) when the parallel bond breaks in the model is given by

$$\tau_p = \frac{\left|F_{t-\Delta t}^s\right|}{A} \tag{11}$$

$$\Delta\tau = \frac{\Delta F_{\Delta t}^s}{A} = -k^s \Delta U^s, \tag{12}$$

where $F_{t-\Delta t}^s$ is the shear loading for an area A as represented in eq. (11). When maximum shear stress is exceeded at (t—Δt), the incremental shear stress ($\Delta\tau$) in eq. (12) is calculated for a time step Δt and shear displacement $\Delta U^s = V_i \Delta t$. The relationship of the plastic viscosity (η) to parallel bond shear stiffness (k^s) is

$$k^s = \frac{\eta}{\Delta t L_0}, \tag{13}$$

where L_0 is the original sample size (Fig. 2b) and V_i is the shear velocity. The parallel bond is regenerated for a viscous fluid as represented by the red particles in Fig. 2(c).

The magma is comprised of silicate melt, crystals and volatiles. The relative proportions of the fractions and their respective compositions exert a significant influence on the magma's bulk composition and its material stiffness. The effect can be parameterized as a function of dissolved water in the melt, crystal content and pressure (Melnik & Sparks 2005). The empirical correlation between liquidus/solidus temperature ($T_{\text{liq,sol}}$) with pressure, obtained from experiments on crystallization of plagioclase feldspar on decompression test for the andesitic magma samples (1996) is given as (Couch *et al.* 2003; Melnik & Sparks 2005)

$$T_{\text{liq,sol}} = a_T + b_T \ln(P) + c_T \ln(P)^2 + d_T \ln(P)^3, \tag{14}$$

where the value of the empirical constants a_T, b_T, c_T and d_T are obtained from the least-squares best fit to the experimental data defined by eq. (14) and listed in Table 2. Lava solidification is related to pressure using the solidus temperature (T_{sol}), which and calculated by eq. (14). Identification of the ductile core-solidified lava interface within the model domain allows material properties to be updated. The failure criterion changes to a Mohr–Coulomb law when the magma transitions from a viscous fluid to a brittle-solid. The Mohr–Coulomb failure criterion in the model is defined as

$$F_s^{\max} = C + \mu_{\text{Friction}} F_n, \tag{15}$$

where $F_s^{\max}$ is the maximum shear force for a specified cohesion (C) and friction coefficient (μ_{Friction}) for a given normal force (F_n). A detailed discussed of the constitutive contact laws that govern particle-particle/wall-particle interaction, parallel bond implementation, factors that control phase change (viscous fluid to brittle solid) and the correlation of contact stiffness with material properties (Young's modulus E and Shear modulus G) are described elsewhere (Husain *et al.* 2014).

Table 2. Constant for the empirical expression obtained for the phase behavior of magma (Melnik & Sparks 2005).

Constant	Liquidus	Solidus
a_T	1465.5	1252.2
b_T	− 31.4	− 25.3
c_T	− 2.8	− 11.9
d_T	− 0.41	1.17

Table 3. Values for the simulation run in Figs 4–7.

Parameter	Value
Density	2500 kg m^{-3}
Solidus Pressure	0.4 MPa
Particle radius	1.5 m
Friction angle (talus)	45°
Linear Contact Stiffness (talus)	2.25×10^8 N m^{-1}
Linear Contact Stiffness (core)	5×10^8 N m^{-1}
Young's Modulus (talus)	3 GPa
Critical crystal volume fraction at onset of yield strength (ϕ_c)	0.2
Maximum volumetric packing fraction of the crystal network in the magma (ϕ_m)	0.9

4 RESULTS AND DISCUSSION

We now evaluate the variation in magma rheology and dome morphology for the range of extrusion rates observed at SHV and MSH. In the following we discuss for SHV the different dome morphologies that may evolve at variable extrusion rates for specified crystal growth rate and magma yield strength. This study is then extended to explore the effects of periodic flow behaviour observed at MSH, USA (1980–1983), with the results discussed in Section 4.2.

4.1 Analysis of dome evolution and the effect of extrusion rate on dome morphology

In this section we develop a model to represent and study the response at SHV, incorporating the effect of crystallization kinetics and list the variation in crystal content of the magma at the conduit vent for nominal values of flow rates ranging between 0.5–8 m^3 s^{-1}. The study considers andesitic magma (bulk composition) with initial crystal content of 0.6 for a magma chamber depth of 5000 m and conduit radius of 15 m (Melnik & Sparks 2005).

The total crystal content in the ascending magma is taken as the sum of the phenocrysts formed in the chamber prior to the eruption, and phenocrysts and microlites that crystallize during magma

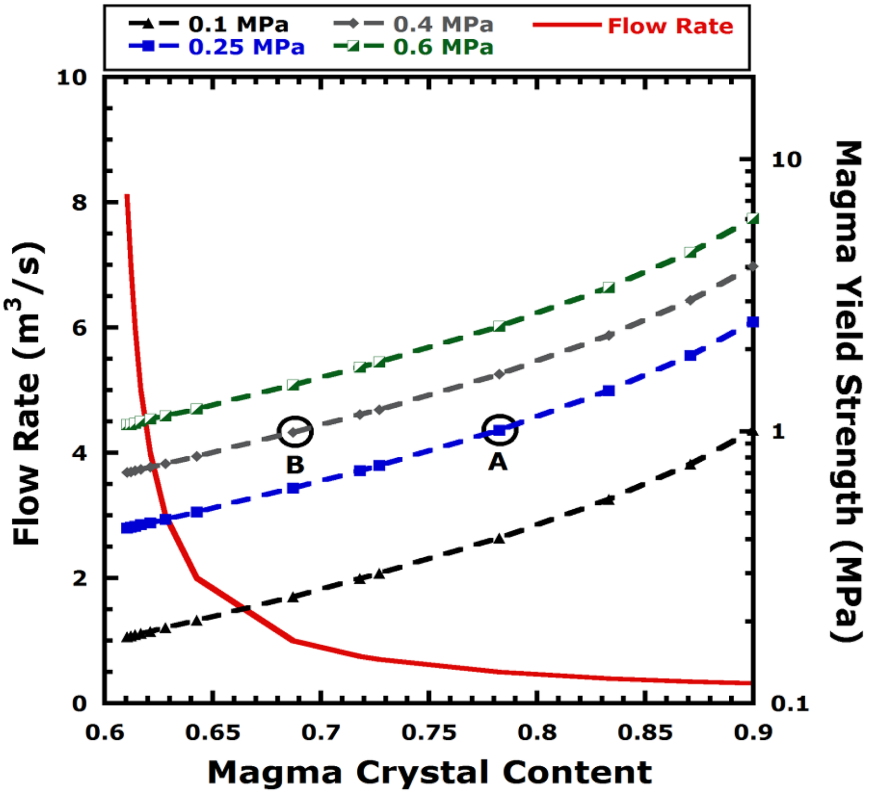

Figure 3. Change in magma crystal volume fraction with decrease in flow rate (solid line) which results in the evolution of yield strength (dash lines) for magma with different values of interparticulate yield strength (τ_0) and linear crystal growth rate of 1.475×10^{-13} m s^{-1}. Points A and B signify locations where the magma yield strength (τ) is 1 MPa for assumed interparticulate resistance (τ_0) of 0.25 and 0.4 MPa, where the crystal volume fractions are 0.78 and 0.69 at flow rates of 0.5 and 0.9 m^3 s^{-1}, respectively.

ascent. In our model we assume that crystal nucleation is instantaneous, which implies that the increment in total crystal content depends solely on the crystal growth rate of the phenocrysts in the magma—a reasonable first order approximation (Marsh 1998; Cashman & Blundy 2000). Eq. (4) illustrates that ascent rate and crystal growth rate influence the magma crystal content during ascent. At lower flow rates (<1 m^3 s^{-1}) the magma is highly crystallized in the upper conduit, and at SHV The crystal volume fraction of the extruded lava, from the shear surfaces of the lava structure, is approximately 0.9 (Sparks *et al.* 2000).

Based on conduit flow modelling, the calculated maximum crystal volume fraction for a magma flow rate of 0.32 m^3 s^{-1} at the conduit exit is $\sim$ 0.9 (Melnik & Sparks 2005). A linear crystal growth rate of 1.475×10^{-13} m s^{-1} is calculated using eq. (16) for our simulations based on the conditions given in the study—with eq. (16) as derived from eq. (4) for a given flow rate. The total crystal content of magma (ϕ) at any given depth is given by

$$\phi^{1/3} = \frac{(36\pi n_{\rm ch})^{1/3} z\chi}{3u} + \phi_{\rm ch}^{1/3}, \qquad (16)$$

where we assume total crystal content is calculated at the vent ($z = L_c$) for a linear crystal growth rate (χ) of 1.475×10^{-13} m s^{-1} and magma crystal content at chamber ($\phi_{\rm ch}$) of 0.6 at different ascent velocities (u). The volume fraction of crystals in the magma increases with a decrease in discharge rate for a specified linear crystal growth rate, magma chamber crystal content and crystal density at a given depth.

Table 3 lists the idealized values considered for magma packets in the simulation runs in the section. Fig. 3 represents the variation in magma crystal volume fraction with flow rate, for the values in Table 3. The increase in crystal volume fraction at low flow rates enhances the yield strength of the extruded magma [which is maintained uniform throughout the lava dome (eq. 7)].

The magma yield strength calculated by Blake (1990) from the reported height and radius of the dacitic MSH (June, 1980) is 0.13 MPa. The stable heights of the extruded spines at SHV suggest that the minimum shear strength of the highly crystalline magma (5–10 per cent melt) was about 1 MPa (Voight *et al.* 1999). In our model, magma yield strength ranges between 0.1 to 6 MPa (Fig. 3), showing the effect of different extrusion rates on yield strength.

The simulations in this section are focused on investigating the effect of crystallization on the flow behaviour of the magma, where the lava dome grows on the rigid horizontal base that is fed through the vent at a constant flow rate. We monitor the variation in morphology of the simulated lava dome at different flow rate intervals ($Q_{\rm out} = 0.5, 2, 4, 6$ and 8 m^3 s^{-1}). Simulation runs are performed for the same set of flow rates for magma with different interparticulate resistances, which governs the non-Newtonian yield strength (τ_p) based on the value of ϕ_c and ϕ_m considered (see eq. 7) ($\tau_0 = 0.10$, 0.25, 0.40 and 0.60 MPa).

In Figs 4 and 5 we compare lava dome morphology of two sets of models with assumed values of $\tau_0 = 0.10$ and 0.25 MPa ($\phi_c = 0.2$ and $\phi_m = 0.9$). Each set is compared for five values of flow rates -0.5, 2, 4, 6 and 8 m^3 s^{-1}, for two simulated eruption times $\sim$4.2 hr (Fig. 4) and 27.8 hr (Fig. 5). The two run times involve 30 000 and 200 000 simulation steps, respectively. The lava dome

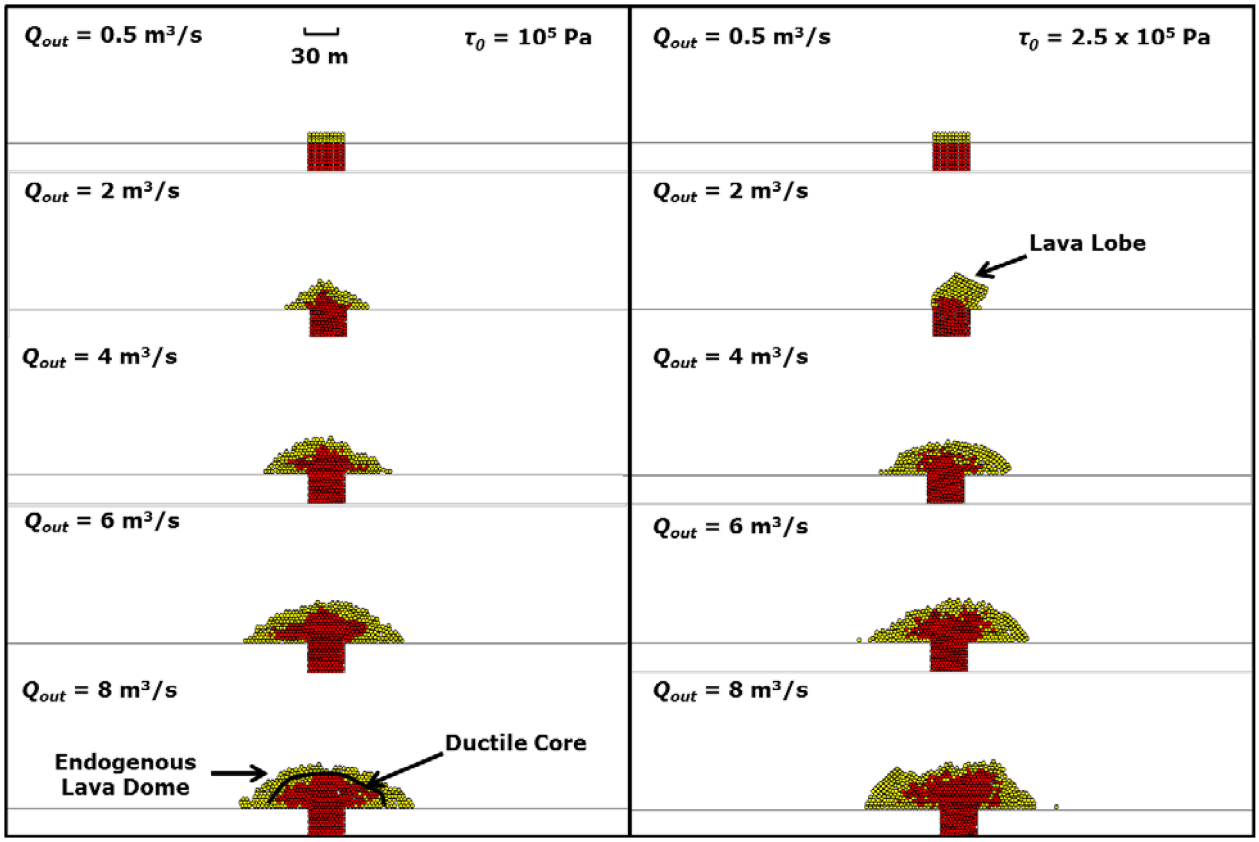

Figure 4. Lava dome morphology of the simulated structure for magma with different assumed interparticulate resistance (constant τ_0 of 0.1 MPa for left side and 0.25 MPa for right side) after $t = 4.167$ hr (30 000 simulation cycles) for a distributed set of specific flow rates ($Q_{out} = 0.5$, 2, 4, 6 and 8 m^3 s^{-1}) where the magma yield strength develops as represented in Fig. 3.

evolves endogenously for the entire range of assumed flow rates (0.5–8 m^3 s^{-1} for constant value of $\tau_0 = 0.1$ MPa), where the magma yield stress (τ) varies for different flow rates (e.g. at 0.5 m^3 s^{-1}, the value of $\phi = 0.8$ with $\tau = 0.4$ MPa represented by Point A in Fig. 4). In the case of constant $\tau_0 = 0.25$ MPa, endogenous growth occurs for flow rates higher than 3 m^3 s^{-1} where τ_p is greater than 0.44 MPa (eq. 7) (at a crystal content of 0.63). For magma with higher yield strength (e.g. with constant interparticle resistance τ_0 of 0.25 MPa) at lower flow rates ($\tau_p = 0.55$ MPa for $\phi = 0.643$ at $Q_{out} =$ 2 m^3 s^{-1}), the unobstructed extrusion of a lava lobe is observed (Point G in Fig. 4).

In Fig. 5, at 27.8 h, a clear distinction occurs between the flow patterns of the two lava domes with different τ_0 values. With $\tau_0 = 0.1$ MPa, the modelled domes remain endogenous for all flow rates (Points A—E in Fig. 5); for these runs the magma yield strength (τ_p) varied from 0.4 MPa ($\phi = 0.782$) at $Q_{out} = 0.5$ m^3 s^{-1} (Point A) to 0.176 MPa ($\phi = 0.61$) at $Q_{out} = 8$ m^3 s^{-1} (Point E). In contrast the simulated lava dome with magma of $\tau_0 = 0.25$ MPa grows endogenously for flow rates greater than about 5 m^3 s^{-1} (Points I and J). The magma yield strength (τ_p) varies from 0.44 MPa ($\phi = 0.61$) at $Q_{out} = 8$ m^3 s^{-1} (Point I) to 0.45 MPa ($\phi = 0.617$) at $Q_{out} = 5$ m^3 s^{-1}. For slightly higher yield strength ($\tau_p = 0.461$ MPa for $\phi = 0.621$) at $Q_{out} = 4$ m^3 s^{-1} (Point H in Fig. 5), the dome structure evolves with the development of shear structures, while there appears to be intermittent exogenous growth (possibly shear lobes) at $Q_{out} = 2$ m^3 s^{-1} ($\tau = 0.51$ MPa for $\phi = 0.643$ given by Point G in Fig. 5). Lower flow rates (<1m^3 s^{-1}) promote greater degassing, which causes stiffer (high yield strength) degassed lava above the conduit vent as observed at $Q_{out} = 0.5$ m^3 s^{-1} ($\tau_p = 1$ MPa for $\phi = 0.782$) (Point F in Fig. 5).

Figs 6 and 7 are similar to Figs 4 and 5 and involve the same range of Q_{out}. The outputs test the influence of different τ_0 values (0.4 and 0.6 MPa) for the same simulation times. In Fig. 6 (t = 4.2 h) the magma extrudes from the vent as a largely-degassed short lava plug for $\tau_0 = 0.4$ and 0.6 MPa ($\tau_p = 1.62$ and 2.43 MPa and $\phi = 0.782$) at $Q_{out} = 0.5$ m^3 s^{-1} (Points A and F in Fig. 6), as observed similarly in Figs 4 and 5. For $Q_{out} = 2$, a spine emerges and rises to greater height commensurate with the Q_{out} increase, but the intact spine is weak and shears ($\tau_0 = 0.4$ MPa) (Point B) or warps $\tau_0 = 0.6$ MPa) (Point G) under the influence of gravity. A domal-shape and endogenous growth occurs for $Q_{out} > 3$ m^3 s^{-1} for magma with $\tau_0 = 0.4$ MPa ($\tau_p = 0.76$ MPa with $\phi = 0.628$), while for the case $\tau_0 = 0.6$ MPa ($\tau_p = 1.09$ MPa with $\phi = 0.6168$) and the same Q_{out}, the spine maintains coherence and although it has partly collapsed or deforms under gravity load, no dome-like form is yet generated. Such a morphology requires $Q_{out} > 5$ m^3 s^{-1}. The yield strength of the lava lobe extruded at $Q_{out} = 4$ m^3 s^{-1} ($\tau_0 = 0.6$ MPa) (Point H) is somewhat weaker than the magma extruded at $Q_{out} = 2$ m^3 s^{-1} (Point G), but in addition twice as much mass has extruded, increasing the spine height and promoting collapse.

In Fig. 7 the simulation times are extended to 27.8 h, and illustrate the further evolution of the dome structures of Fig. 6. For $Q_{out} <$ 5 m^3 s^{-1}, the increase in magma yield strength leads to intermittent exogenous growth, with spines pushing out of the dome, or, for $\tau_0 = 0.6$ MPa, shear lobes for $Q_{out} = 2$–4 m^3 s^{-1} (Points G and

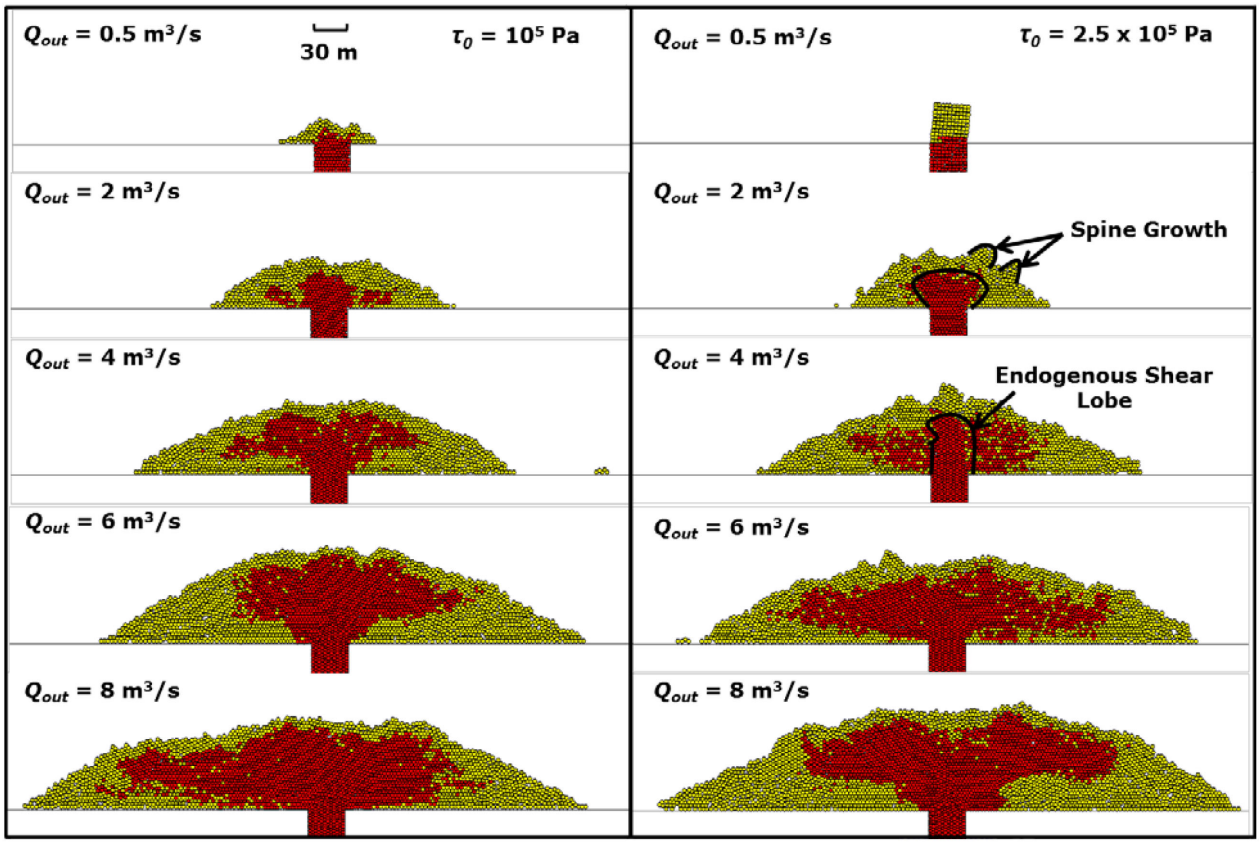

Figure 5. Lava dome morphology of the simulated structure for magma with different assumed interparticulate resistance ($\tau_0 = 0.1$ MPa for left side and 0.25 MPa for right side) after $t = 27.778$ hr (200 000 simulation cycles) for a distributed set of specific flow rates ($Q_{out} = 0.5$, 2, 4, 6 and 8 m^3 s^{-1}) where the magma yield strength develops as represented in Fig. 3.

H). At higher flow rates ($Q_{out} > 5$ m^3 s^{-1}) and for $\tau_0 = 0.6$ and 0.4 MPa, growth appears endogenous with development of a ductile core and approximately parabolic external form (Points D, E, I and J in Fig. 7).

Magma rheology can change from (approximately) Newtonian to Bingham upon the formation of a continuous crystal network and the development of a finite yield strength that increases rapidly with increase in crystal volume fraction (Saar *et al.* 2001). Such a change in the magma rheology can result in the transition from endogenous growth of low-yield strength magma to exogenous high-yield strength spine extrusion. The transition is principally controlled by the extrusion rate as this affects magma crystallization and defines the enhancement in yield strength.

The lava dome will grow endogenously and without the development of shear lobes, for magma yield strengths lower than 1 MPa (represented by Points A and B in Fig. 3, for $\tau_0 = 0.25$ and 0.4 MPa and for flow rates greater than $\sim$5 m^3 s^{-1}). In the case of higher yield strength ($\tau_p > 1$ MPa) returned at lower flow rates ($Q_{out} <$ 1 m^3 s^{-1}), an exogenous extrusion of a degassed lava plug results (Points A and F in Fig. 7). Intermediate behaviour such as evolution of an endogenous shear lobe depends on the combination of magma yield strength and extrusion rate, which can vary between $\tau_p = 0.46$ MPa (for $\tau_0 = 0.25$ MPa), Point H in Fig. 5, to $\tau_p = 1.11$ MPa (for $\tau_0 = 0.6$ MPa), Point H in Fig. 7, at 4 m^3 s^{-1}.

The effect of extrusion rate on magma rheology is significant, and includes its effect on periodic extrusion (Denlinger & Hoblitt 1999; Barmin *et al.* 2002; Huppert & Woods 2002; Melnik & Sparks 2002, 2005, 1999; Voight *et al.* 1999). The amplitude of the extrusion rate and the periodicity of the eruption cycles are affected by magma chamber and conduit system constraints, including size, depth, conduit dimensions and shape (Costa *et al.* 2007), rigidity of the wall rock and rate of replenishment in chamber and back pressure of growing dome (Watts *et al.* 2002; Hale 2008). In the subsequent section we discuss the effects of these parameters on the lava dome morphology by coupling conduit flow mechanics with the particle-mechanics model which represents surface deformation.

4.2 Controls on flow transition from endogenous growth to exogenous spine evolution

In this section we investigate the periodic behaviour observed during the lava dome eruptions at MSH (1980–1983). In the eruption of MSH in 1980–1986 more than 20 short episodes of dacite dome growth, lasting 2–7 d, alternated with longer periods of no growth (Swanson & Holcomb 1990). There were two sequences of periodic dome growth, with an intervening episode of near-continuous dome growth lasting 368 d (Swanson & Holcomb 1990).

Barmin *et al.* (2002) had developed a generic model of magma discharge through a conduit from an open-system magma chamber with continuous replenishment, considering the principal controls on flow, namely the replenishment rate, magma chamber size, elastic deformation of the chamber walls, conduit resistance, and variations of magma viscosity controlled by degassing during ascent and kinetics of crystallization. Their analysis included MSH and indicated a rich diversity of behaviour with periodic patterns similar to those

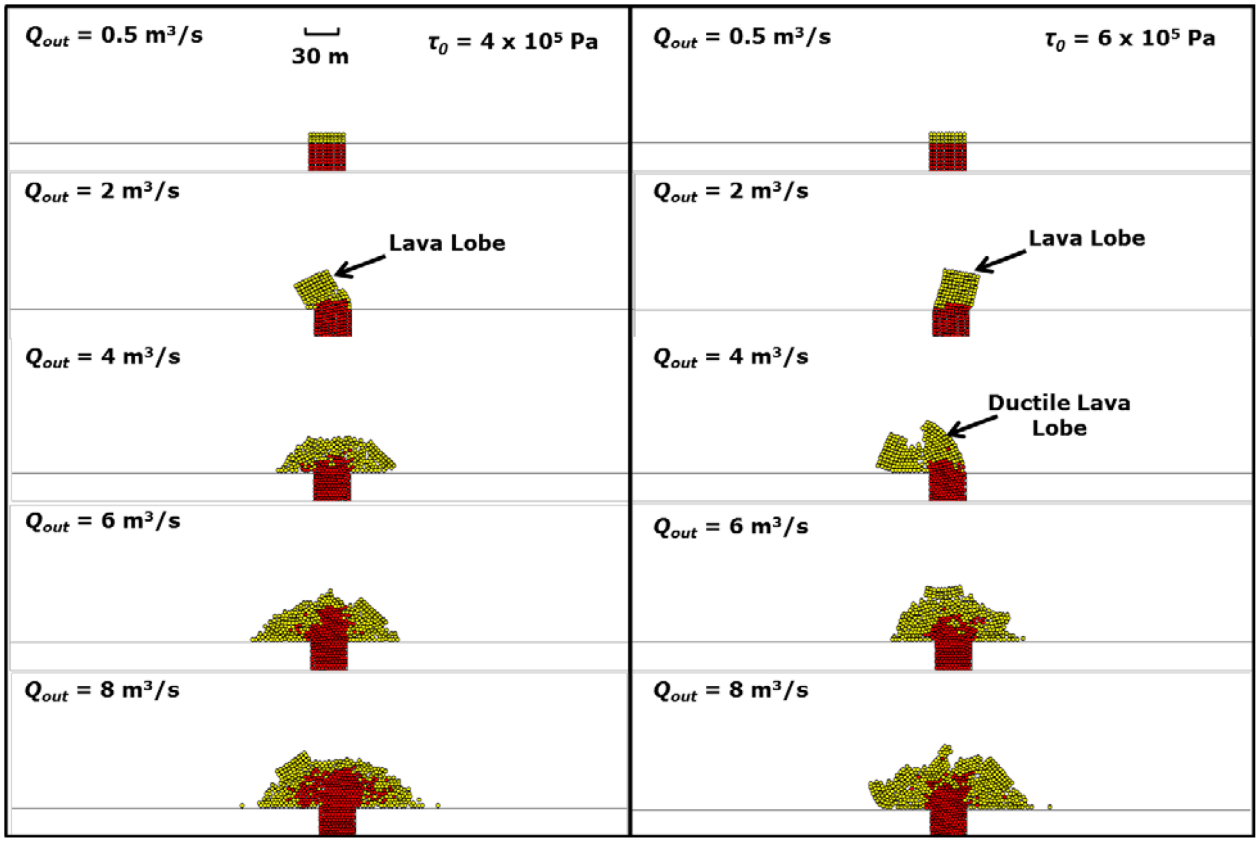

Figure 6. Lava dome morphology of the simulated structure for magma with different assumed interparticulate resistance ($\tau_0 = 0.4$ MPa for left side and 0.6 MPa for right side) after $t = 4.167$ hr (30 000 simulation cycles) for a distributed set of specific flow rates ($Q_{out} = 0.5$, 2, 4, 6 and 8 m^3 s^{-1}) where the magma yield strength develops as represented in Fig. 3.

observed at several other volcanoes. They noted that magma chamber size might be estimated from the period, with longer periods implying larger chambers.

In our analysis we adopt, with a few exceptions, the parameters adopted for the calculation of magma ascent by Barmin *et al.* (2002). The values inferred by Barmin *et al.* (2002) are based on the match obtained with the lava dome eruption data for MSH presented by Swanson & Holcomb (1990). We use the parameters in Table 4. The viscosity ratio (μ_2/μ_1), which controls the period of oscillation and magnitude of flow rate (section between Y_1 and Y_2), is taken as 52.7, instead of 80 (Barmin *et al.* 2002). The replenishment rate (Q_{in}) inferred in the study by Barmin *et al.* (2002) is 0.67 m^3 s^{-1}, and is set at 0.75 m^3 s^{-1} in our simulation. The magma chamber volume (V_{ch}) is set at 0.1 km^3 in most our simulations, smaller than the Barmin *et al.* (2002) best-fit value of 0.56 km^3. We choose this lower volume to reduce the execution time for the model. For a closed system, the duration of the eruption should scale with the volume of the chamber. Reducing the volume by a factor of ∼6 should decrease the duration of the eruption by that order. In this particular case the observed period of oscillation of the discharge pulse thus reduces from ∼70 d (as observed at MSH) to 1.5 d (this model) representing a change in duration slightly larger than this factor of ∼6 (at ∼50). This is likely due to the impact of the nonlinear response of the system. The intentional reduction in the viscosity ratio, replenishment rate and magma chamber volume from the values considered by Barmin *et al.* (2002) aids in reducing the duration of eruption, while maintaining the peak flow rate (∼12 m^3 s^{-1}), which assists in decreasing the simulation time significantly. These model choices have been made to accelerate the computation with the results demonstrating the style of cyclicity and its control on the resulting dome morphology. Our principal objective is to establish that our model can generate a *style* of periodic behaviour similar to that observed at MSH, but it is not our intent to attempt to reproduce the periodicity exactly. Regarding chamber volume, the best-fit value determined by Barmin *et al.* (2002) was unrealistically small. The total DRE volume erupted in 1980–86 is about 0.6 km^3, and the corresponding chamber volume is likely an order of magnitude greater—for example, Mastin *et al.* (2008) suggested at least several to a few tens km^3. Thus their result is incorrect by an order of magnitude, which probably reflects simplifications introduced in their generic models, and parameter choices.

The peak discharge rate at MSH during the eruption period from 1981–1982 is ∼12 m^3 s^{-1}. The magma chamber depth (L_c) is estimated at ∼7200 m (Pallister *et al.* 1992).The crystal density per unit volume (n_{ch}) at chamber conditions is set as 10^{14} m^{-3}, consistent with the observations of microphenocrysts in the lava samples from the dome eruptions of 1980–1986 (Cashman & Blundy 2000). The crystal content in the magma chamber (ϕ_{ch}) is taken at 30 per cent, and assuming a rhyolitic melt at 900° C with 5 wt per cent H_2O (Cashman & Blundy 2000), the estimated chamber viscosity is 6.4×10^4 Pa.s (Barmin *et al.* 2002). Following Barmin *et al.* (2002), the average lower conduit magma viscosity is taken as 10 times higher than chamber viscosity, which is $\mu_1 = 6.4 \times 10^5$ Pa.s. Above the transition depth, we use $\mu_2 = 3.38 \times 10^7$ Pa.s, using Barmin *et al.* (2002) initial estimate of viscosity ratio of 52.7 instead of their best-fit value of 80. The conduit radius (r_c) is estimated at 10 ± 2.5 m

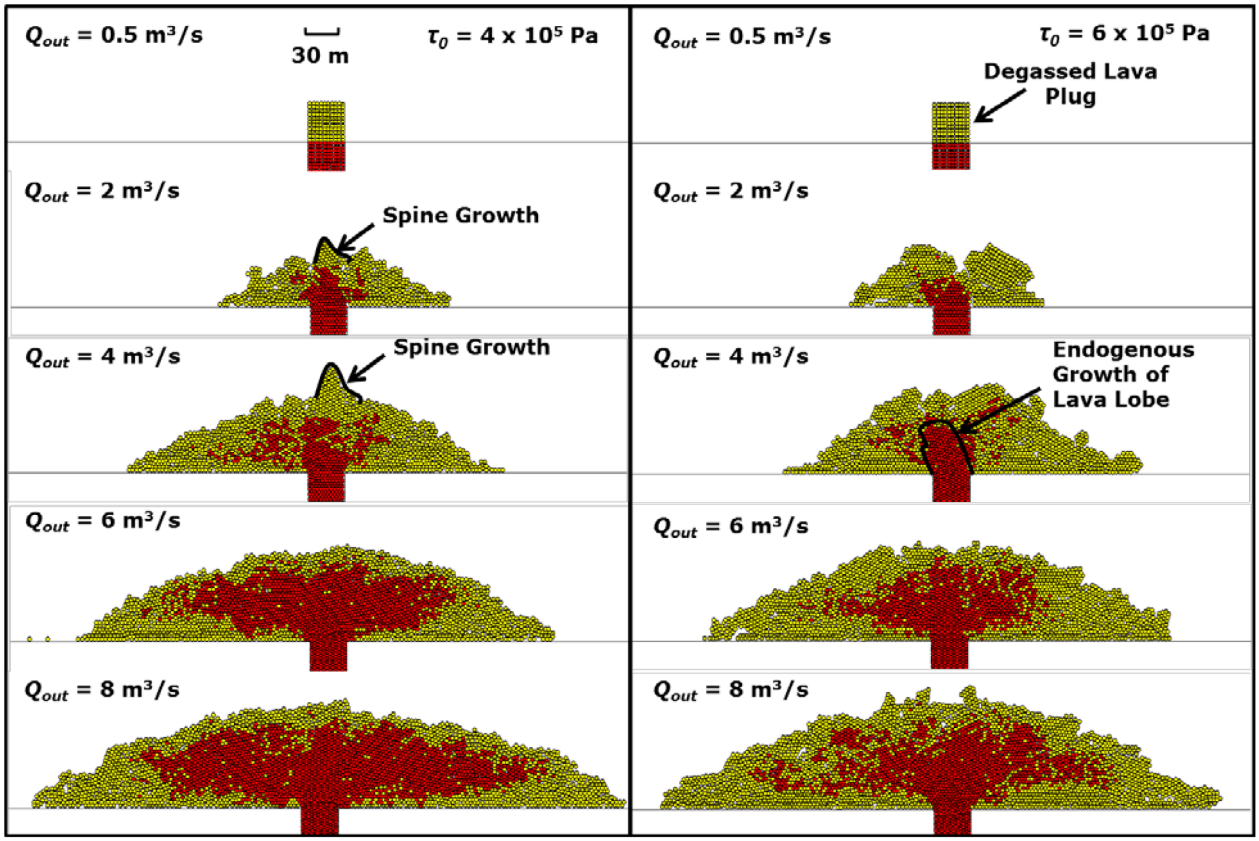

Figure 7. Lava dome morphology of the simulated structure for magma with different assumed interparticulate resistance ($\tau_0 = 0.4$ MPa for left side and 0.6 MPa for left side) after $t = 27.778$ hr (200 000 simulation cycles) for a distributed set of specific flow rates ($Q_{out} = 0.5$, 2, 4, 6 and 8 m^3 s^{-1}) where the magma yield strength develops as represented in Fig. 3.

Table 4. Parameters used for modelling the style of the Mount St Helens lava dome eruptions (from Barmin *et al.* (2002) except as noted in the text.

Parameter	Value
μ_1	6.4×10^5 Pa s
μ_2	3.34×10^7 Pa s
ρ	2500 kg m^{-3}
L_c	7200 m
r_c	9 m
ϕ_{ch}	0.3
ϕ_T	0.7
Q_{in}	0.75 m^3 s^{-1}
n_{ch}	10^{14} m^{-3}
χ	1.475×10^{-12} m s^{-1}
V_{ch}	0.1 km^3

from observation of the October 1980 dome, and also from ascent velocities based on amphibole reaction rims (Anderson & Fink 1990; Swanson & Holcomb 1990; Rutherford & Hill 1993). The conduit radius (r_c) is set at 9 m. The crystal content at which the transition in the viscosity occurs, is assumed at $\phi_T = 0.7$ for a crystal growth rate (χ) of 1.475×10^{-12} m s^{-1}. The remaining parameters in the simulation are maintained constant as listed in Table 4. The notation and dimensions for all variables are listed in Table 5.

Fig. 8 shows the variations in periodic behaviour for two different assumed chamber volumes 0.1 and 0.56 km^3. Note that the periodicity is about 1.5 d for a chamber volume of 0.1 km^3, and about 9 d for a volume of 0.56 km^3, demonstrating the sensitivity of period on assumed chamber volume. For each case we also demonstrate that the analytical solution results can be matched by the particle-mechanics modelling. Thus the style of periodicity in our models successfully matches the general style of periodicity observed at MSH (see e.g. Barmin *et al.* 2002; Fig. 5a). However the lengths of period observed in our models are shorter than at MSH, due to our need to adjust parameters to shorten the calculation run times. Multiple runs are made for the pair of different values of viscosity ratio, replenishment rate and magma chamber volume to obtain the optimum possible simulation run time and minimum deviation from the values obtained in the study by Barmin *et al.* (2002).

For the particle-mechanics model, the evolution of yield strength (τ_p) with flow rate due to the change in magma crystal content is shown in Fig. 9. Magma yield strength increases with an increase in crystal content and is larger at lower flow rates due to greater loss of volatiles. The effect of crystallization on bulk viscosity, coupled with magma replenishment to the chamber, creates a cyclic pattern between chamber pressure and flow rate. Fig. 10 shows the cyclic behaviour for the assumed chamber volume of 0.1 km^3.

The steady state solution in Fig. 10 is divided into 3 parts, comprising the flow regime above X_2, the section between X_2 and X_1 and the region below X_1. Flow rates greater than X_2 (Fig. 10) are characterized by the extrusion of magma with lower crystal content, which results in lower magma bulk viscosity. The conduit resistance for flow rates smaller than X_1 is larger due to the relatively high viscosity for magma with higher crystal content. The nature of

Table 5. Notation.

Parameter	Description	Unit
P	Magma Density	$M^1\ L^{-3}$
T	Time	T^1
U	Flow Velocity	$L^1\ T^{-1}$
Z	Distance in the vertical direction	L^1
N	Crystal density per unit volume of magma	L^{-3}
Ch	Subscript for magma chamber	–
P	Pressure	$M^1\ L^{-1}\ T^{-2}$
G	Acceleration due to gravity	$L^1\ T^{-2}$
μ	Magma viscosity	$M^1\ L^{-1}\ T^{-1}$
r_c	Conduit radius	L^1
μ_1	Magma viscosity below the transition depth	$M^1\ L^{-1}\ T^{-1}$
μ_2	Magma viscosity above the transition depth	$M^1\ L^{-1}\ T^{-1}$
Φ	Magma crystal content	–
ϕ_T	Magma crystal content at transition depth	–
X	Linear crystal growth rate	$L^1\ T^{-1}$
Γ	Rigidity of the surrounding wall rock	$M^1\ L^{-1}\ T^{-2}$
V_{ch}	Magma chamber volume	L^3
Q_{in}	Magma replenishment flow rate	$L^3\ T^{-1}$
Q_{out}	Magma flow rate through conduit exit	$L^3\ T^{-1}$
L_{c}	Magma chamber depth	L^1
τ_0	Interparticulate resistance to hydrodynamic forces (Saar *et al.* 2001).	$M^1\ L^{-1}\ T^{-2}$
τ_p	Yield strength of a non-Newtonian fluid	$M^1\ L^{-1}\ T^{-2}$
ϕ_c	Critical crystal volumetric fraction at onset of magma yield strength	–
ϕ_m	Maximum packing volumetric fraction of a crystal network in magma; this determines the transition to a solid	–
T	Shear stress	$M^1\ L^{-1}\ T^{-2}$
η	Non-Newtonian plastic viscosity	$M^1\ L^{-1}\ T^{-1}$
$\dot{\gamma}$	Strain Rate	T^{-1}
η_{app}	Apparent viscosity of non-Newtonian fluid	$M^1\ L^{-1}\ T^{-1}$
F_t^s	Shear force exerted at a given time step (t)	$M^1\ L^1\ T^{-2}$
Δt	Timestep	T^1
A	Effective area on which shear load is applied	L^2
$\Delta\tau$	Difference in shear stress over a given time step (Δt)	$M^1\ L^{-1}\ T^{-2}$
k^s	Parallel bond shear stiffness	$M^1\ L^{-2}\ T^{-2}$
ΔU^s	Shear displacement for a given time step Δt	L^1
V_i	Shear velocity for the given time step Δt	$L^1\ T^{-1}$
L_0	Original length of the sample/particle	L^1
T_{liq}	Temperature of the magma in the liquid state	–
T_{sol}	Temperature of the magma in the solid state	–
H	Lava dome height	$M^0\ L^1\ T^0$
F_n	Applied normal force	$M^1\ L^1\ T^{-2}$
a_T	Constant for the empirical expression to obtain the phase behavior of the magma at Soufrière Hills Volcano, Montserrat	–
b_T	Constant for the empirical expression to obtain the phase behavior of the magma at Soufrière Hills Volcano, Montserrat	–
c_T	Constant for the empirical expression to obtain the phase behavior of the magma at Soufrière Hills Volcano, Montserrat	–
d_T	Constant for the empirical expression to obtain the phase behavior of the magma at Soufrière Hills Volcano, Montserrat	–
$F_s^{\max}$	Maximum applied shear force	$M^1\ L^1\ T^{-2}$
C	Cohesion in Mohr–Coulomb failure criterion	$M^1\ L^{-1}\ T^{-2}$
μ_{Friction}	Coefficient of friction of the material	–
F_n	Applied normal force	$M^1L^1T^{-2}$
h	Lava dome height	$M^0L^1T^0$

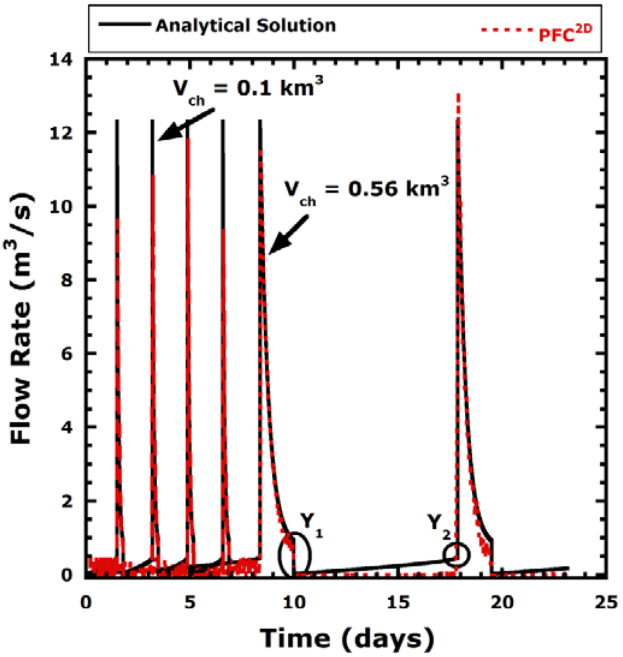

Figure 8. Periodic discharge of magma (solid line) from an analytical solution of a pressurized magma chamber with different volumes ($V_{ch} = 0.1$ and 0.56 km^3) simulated with parameters mainly inferred for Mount St. Helens (1980–1983). The parameters for the simulation are listed in Table 4. The dashed lines are the calculated flow data from the 2-D model developed in the particle-mechanics code for an evolving lava dome. Points Y_1 and Y_2 indicate the transition in flow rate where the flow rate drops and rises due to the variation in magma viscosity. The periodicity for chamber volume of 0.1 and 0.56 km^3 is 1.5 and 9 d, respectively.

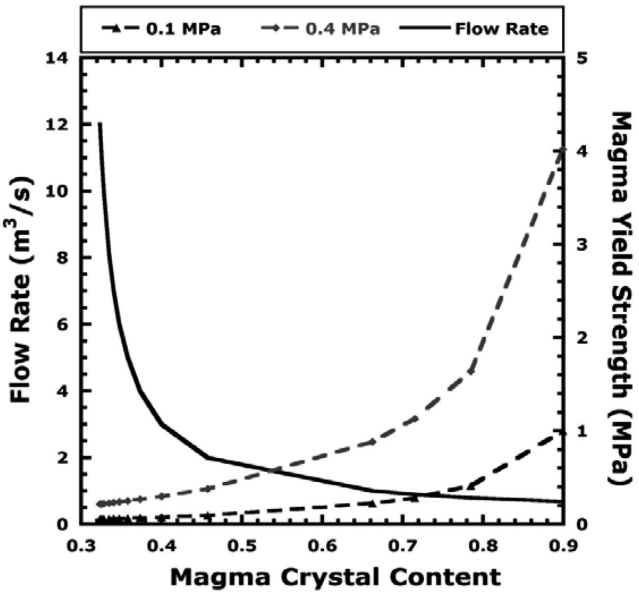

Figure 9. Change in magma crystal content with flow rate (solid line), for range of flow rates expressed in Fig. 8. The changing crystal content with magma flow rate results in the evolution of yield strength (dash lines) for magma with different assumed values of interparticulate resistance (τ_0) and linear crystal growth rate of 1.475×10^{-12} m s^{-1}.

the periodic behaviour (duration of the pulse and time difference between successive pulses) is governed by the value of Q_{in}. For values of Q_{in} greater than X_2 and smaller than X_1, Q_{out} stabilizes with time. If Q_{in} is between X_1 and X_2, then a periodic behaviour as represented by Fig. 8 is observed (Barmin *et al.* 2002; Melnik & Sparks 2005). The drop in flow rate labelled as Point Y_1 in Fig. 8 is influenced by the values of X_1 and X_2, which govern the nature of the flow regime from $Q_{in} = 0$ to $Q_{in} = X_2$.

Fig. 11 illustrates the variation in magma crystal content at the conduit exit and the resulting evolution of yield strength for the flow history shown in Fig. 8. Particle-mechanics simulations using parameters in Table 3 were performed for magma with different assumed interparticulate resistance ($\tau_0 = 0.1$ and 0.4 MPa). The variations in magma yield strength for the flow rates specified in Fig. 8 are linked to the snapshots (labelled A—J) in Figs 12 and 13. These figures show the simulated dome morphologies at selected times during the first four flow pulses, with the left and right panels using different assumed values of interparticulate resistance (τ_0).

The magma rheologies are manifest in the dome morphology of the simulated lava domes. In principle, comparisons could be made to field observations linked to observed extrusion rates (Figs 8, 10, 12 and 13).

In Fig. 12, the initial flow rate is low due to resistance of the high-viscosity, degassed and highly crystalline magma in the upper section of the conduit. Following extrusion, the flow rate peaks at $\sim$12 m^3 s^{-1}. Point A in Fig. 11 represents post-extrusion of the plug and low yield strength magma at high flow rate, which generates endogenous dome growth (Point A in Fig. 12, for $\tau_0 = 0.1$ MPa). The extrusion rate drops (Fig. 8) as ascending magma crystallizes (Fig. 11), increasing bulk viscosity. The erupting pulse of relatively low-crystal fraction magma ends at 1.75 d (pulse duration 0.25 d) initiating regeneration of a viscous plug in the upper conduit. The viscous plug is extruded at a low flow rate ($Q_{out} \sim 0.34$ m^3 s^{-1}) leading generation of an internal shear lobe, Point B in Fig. 12.

With each pulse of extruded magma, the chamber pressure decreases and reaches the value represented by X_2, subsequently ramping up to X_1 with replenishment of the magma chamber (Fig. 10). The extrusion rates drop with development of a conduit plug (Fig. 10). Following plug extrusion, lower-viscosity magma is infused into the lava dome resulting in endogenous dome growth, Point C (t = 3.3 d, $Q_{out} \sim 3.15$ m^3 s^{-1}). The dome evolves in a similar repetitive manner for the recurring cycles of eruption, with the right-hand panels showing more mound-like protrusions in dome morphology, reflecting locally stiffer magma and perhaps the surface expression of more-coherent shear lobes.

Following the third pulse, an exogenous spine has developed in the higher-strength magma, punching through the dome surface with a push from underlying low-viscosity magma (Point E, Fig. 13). The next pulse follows the same pattern, with a stiff spine developing endogenously at low flow rates (Point G, Fig. 13), which topples to the dome surface (Point H, Fig. 13). The extrusion of the toppled spine is aided by a push by low-viscosity conduit magma (Points I, J in Fig. 13).

The magma rheologies are manifest in the dome morphology of the simulated lava domes. In principle, comparisons could be made to field observations linked to observed extrusion rates (Figs 8, 10, 12 and 13), being mindful of the difference between our simulation periodicity of 1.5 d and the 70 d periods typically observed at MSH (Swanson & Holcomb 1990).The typical dome configurations bear many similarities to MSH observations, where surface textures changed with time and degree of movement, becoming rougher and exhibiting mounds and occasional short-lived spines (Moore *et al.* 1981; Anderson & Fink 1990).

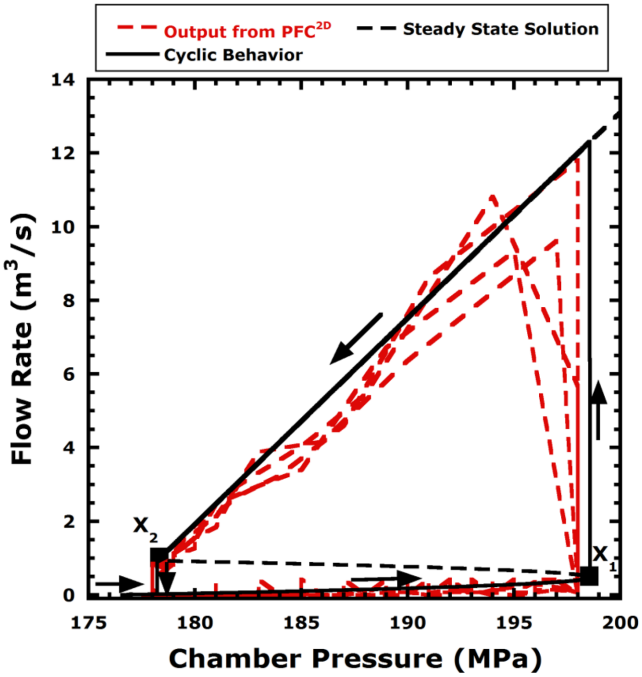

Figure 10. Cyclic behavior of magma chamber pressure with flow rate for the flow rate history in Fig. 8 ($V_{ch} = 0.1$ km^3) (solid line) (Barmin *et al.* 2002). The steady state solution is indicated by the black dashed line and Points X_1 and X_2 correspond to Points Y_2 and Y_1 in Fig. 8 respectively. The Points X_1 and X_2 indicate the transition pressures where there is an unsteady change in flow rate due to variation in magma viscosity. The red dashed line indicates the calculated flow data from the 2-D particle-mechanics model using the same assumptions, for an evolving lava dome.

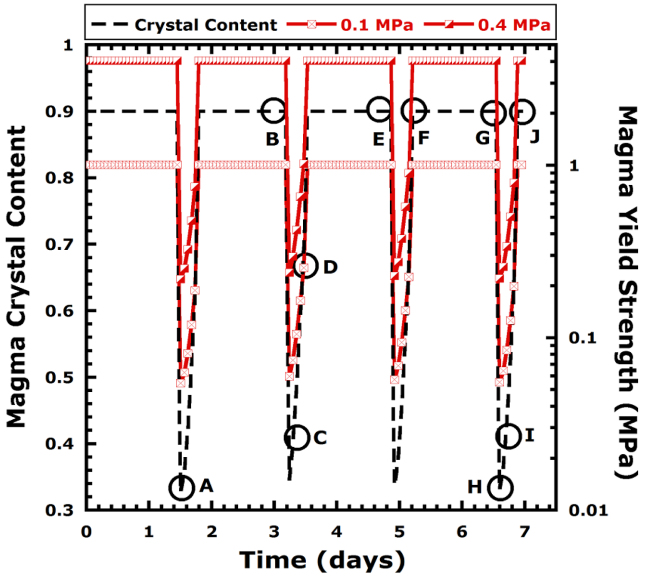

Figure 11. Variations in crystal content at specific times are indicated by Points A—J (dashed line). The resulting change in yield strength for magma is mapped for different assumed interparticulate resistance ($\tau_0 = 0.1$ (dashed red line) and 0.4 MPa (solid red line)) for the flow rate history given in Fig. 8.

One measure of average dome shape is the height–depth (h/d) aspect ratio, and for the MSH composite domes between December 1980 and late 1986, the range of h/d ratios was 0.23 to 0.29, with the mean about 0.27 (Swanson & Holcomb 1990). The earlier data between December 1980 and April 1981 suggested the range 0.23–0.25.

In comparison, the post-pulse simulations (snapshots B, E, G, J; Figs 12 and 13) give h/d ratios of 0.21, 0.20, 0.18, 0.19 for the four low-strength pulses, and 0.25, 0.23, 0.24 (0.18 without spine), 0.23 for the high-strength pulses. Two values are given for the G high-strength snapshot, the first equating dome height with the height of spine, and the second on overall dome height discounting the spine. Overall the latter group matching best with the MSH field data.

An interesting result from our simulations is that the dome aspect ratio changes with time, indicating sagging and spreading. This is shown for h/d between post-pulse 2 snapshots D and E (0.22 → 0.20, and 0.26 → 0.23, respectively for low-strength and high-strength cases. Similarly, for post-pulse 3, snapshots F and G show 0.23 → 0.18 for the low-strength case, and 0.27 → 0.24 (with spine) and 0.21 → 0.18 (discounting spine) for the high-strength case. The sagging actually starts while the pulse is in progress, as shown for pulse 4, where Point I gives geometry near the peak of pulse, and Point J represents pulse termination (Figs 10 and 13); the ratio changes are 0.22 → 0.19, 0.23 → 0.22 for the two strength cases, with further adjustments aborted by run termination. These changes are observed visually in Figs 12 and 13, indicated by reduced dome heights and broadened diameters, and by flattening or depressing of the dome top (e.g. a depression is shown in low-strength J in Fig. 13).

Field observations at MSH confirm the occurrence of such phenomena. Particularly good documentation is given by Moore *et al.* (1981) for the dome which began growth on the afternoon of October 18. The dome was first observed an hour after the last of a series of explosions that occurred between October 16 and 1428 October 18 (Moore *et al.* 1981). At 1520 a new dome was observed, about 5 m high and 25 m across. An hour later it was 10 m high and 40 m wide, and by 0925 on October 19 the dome was subcircularin plan with a radius of 92.5 m and a height of 50 m. The surface was convex-upward, cut by deep cracks with incandescent walls. Theodolite measurements were initiated at 1030 on 19 October and documented changes in shape and dimensions over the next several days (Moore *et al.* 1981):

> The dome subsided more than 18 m and widened more than 15 m (in some places more than 19 m) between October 19 and 27. These changes took place at a rate of ~2.1 m hr^{-1} on October 19 which nearly stopped by October 27. During this period, the shape of the dome changed markedly and finally acquired a nearly flat top with a small depression near its centre. Large cracks, as deep as 5–7 m, radiated from this depression similar to spokes on a wheel. A single spire rose 3–4 m above the general surface.

The final diameter (27 October) of the subcircular dome was about 225 m, with its height above the crater floor about 37 m. From these data the h/d ratio is about 0.16, reduced in 8 d from approximately 0.27 on October 19. This ratio change is similar to our simulation results, making allowance for the additional time over which subsidence occurred at MSH.

The change can be attributed to gravitational spreading facilitated by a viscous dome interior with movements limited by magma yield strength and talus friction resistance, and degassing of the dome core and magma column. Similar morphologic changes with dome-top subsidence have been reported elsewhere such as at Merapi in Java (Voight *et al.* 2000).

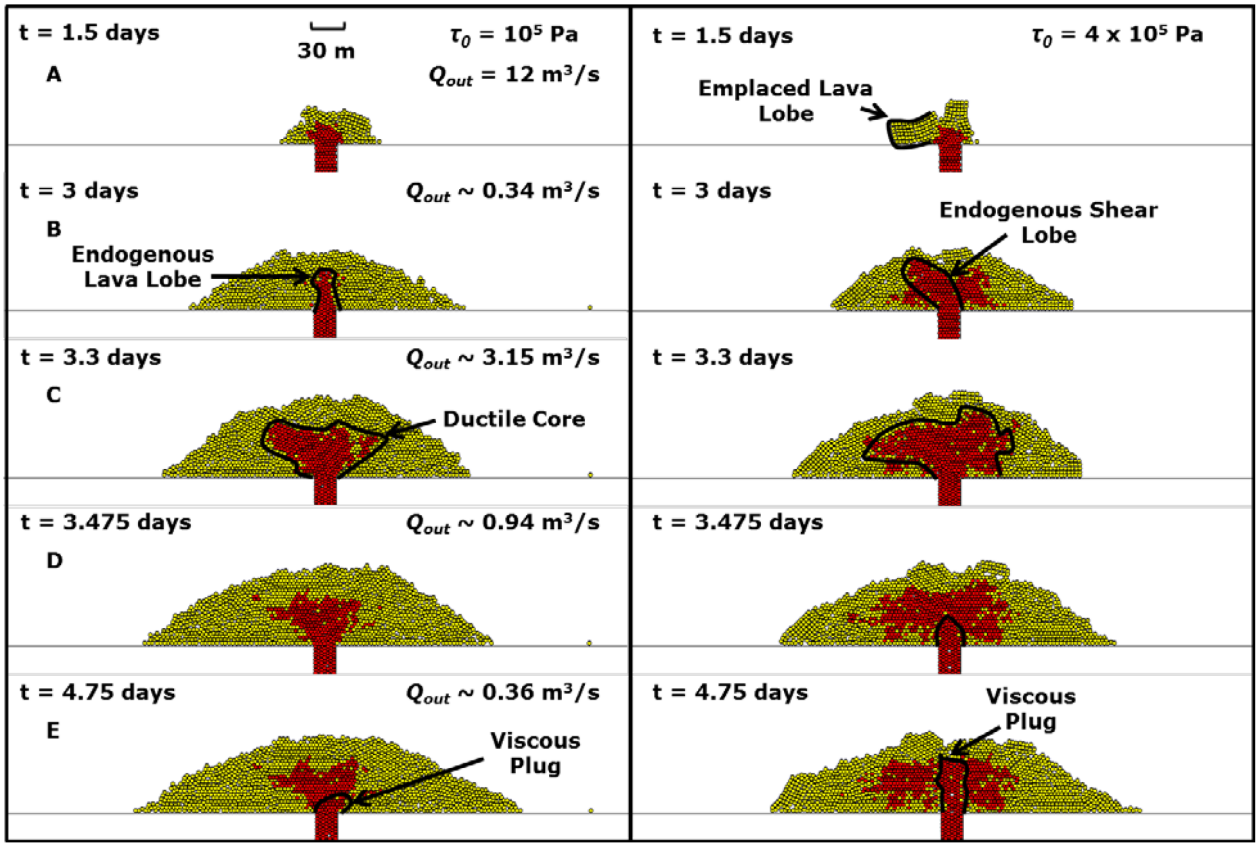

Figure 12. Snapshots of the simulated lava dome morphology for the flow rate history given in Fig. 8. The time intervals at which the snapshots were taken correspond with the labels in Fig. 11 which provide the magnitude of the extruding magma yield strength due to change in crystal content with the periodic flow rate history given in Fig. 9. The simulations are performed for magma with different interparticulate yield strength ($\tau_0 = 0.1$ and 0.4 MPa) with the corresponding snapshots represented above taken at 1.5, 3, 3.3, 3.475 and 4.75 d during the eruption cycle.

Moore *et al.* (1981) proposed that the initiation of subsidence probably reflects the cessation of extrusion and the stagnation of the magma column, and while these factors are important to sagging and spreading, our simulations show that the process can start even before extrusion shuts down (snapshots I, J; Fig. 13).

The low aspect ratio (h/d) for the MSH lava dome of October 1980, may suggest a thin crust overlying a hot interior (Swanson & Holcomb 1990) and strength even less than for our low-strength model. The main explanation may be that this extrusion followed on the heels of an explosive eruption, without time for a conduit plug to develop. An alternative explanation is that this magma was slightly more mafic and thus of lower viscosity (Lipman *et al.* 1981), but this difference in chemistry is not confirmed by Cashman & Taggart (1983).

4.3 Flow rate controls on growth styles

Observations at volcanoes such as SHV and MSH indicate that specific dome growth styles occur for specific ranges of flow rates (Blake 1990; Griffiths & Fink 1997; Stasiuk & Jaupart 1997; Griffiths 2000; Sparks *et al.* 2000; Watts *et al.* 2002; Cashman *et al.* 2008; Hale & Wadge 2008; Mastin *et al.* 2008; Anderson & Segall 2011). New magma is supplied to the dome periodically from the magma chamber as pulses, and push out conduit plugs that developed from rheological stiffening at low flow rates, due to degassing induced crystallization. The plug develops at low flow rates (values below X_1, Fig. 10) and slowly extrudes, Points B, E in Fig. 12; Point G, Fig. 13.

The extent of rise of the viscous plug within the dome structure is governed by the rate at which flow rate increases in the region below X_1 in Fig. 10. The rate of change of flow rate with chamber pressure is governed by the viscosity ratio μ_2/μ_1, the volume of the magma chamber and the magma yield strength for specified values of ϕ and ϕ_T representing a magma chamber at a given depth. The ratio μ_2/μ_1 defines the magnitude of the increase of flow rate with time, while the volume of the magma chamber controls the duration for which the flow rate remains below X_1. For a smaller magma chamber volume and lower ratio of μ_2/μ_1 the value of X_1 is greater and is reached at a faster rate, which results in a smaller magma plug with lower viscosity. A stiffer, more degassed plug is extruded for a longer time, for a larger magma chamber with a higher μ_2/μ_1 ratio.

The viscous plug can extrude exogenously as a spine of solidified magma, but for lower yield strength it is more prone to remain within the dome as an endogenous element. Point F in Fig. 13 illustrates that magma with $\tau_0 = 0.4$ MPa exhibits exogenous spine growth and endogenous for $\tau_0 = 0.1$ MPa. Exogenous growth is observed at flow rates (Q_{out}) < 2 m^3 s^{-1} for $\tau_0 > 3 \times 10^5$ Pa, while for higher flow rates ($2 < Q_{\text{out}} < 12$ m^3 s^{-1}), endogenous growth of a ductile core occurs, e.g. Point C, Fig. 12 and Point I, Fig. 13.

Point Y_1 in Fig. 8 plays a crucial role in determining the growth of a viscous plug. A lower value ($Q_{\text{out}} < 2$ m^3 s^{-1} for $\tau_0 = 0.4$ MPa) of X_2 in Fig. 10, represented by Point Y_1 in Fig. 8, results in the

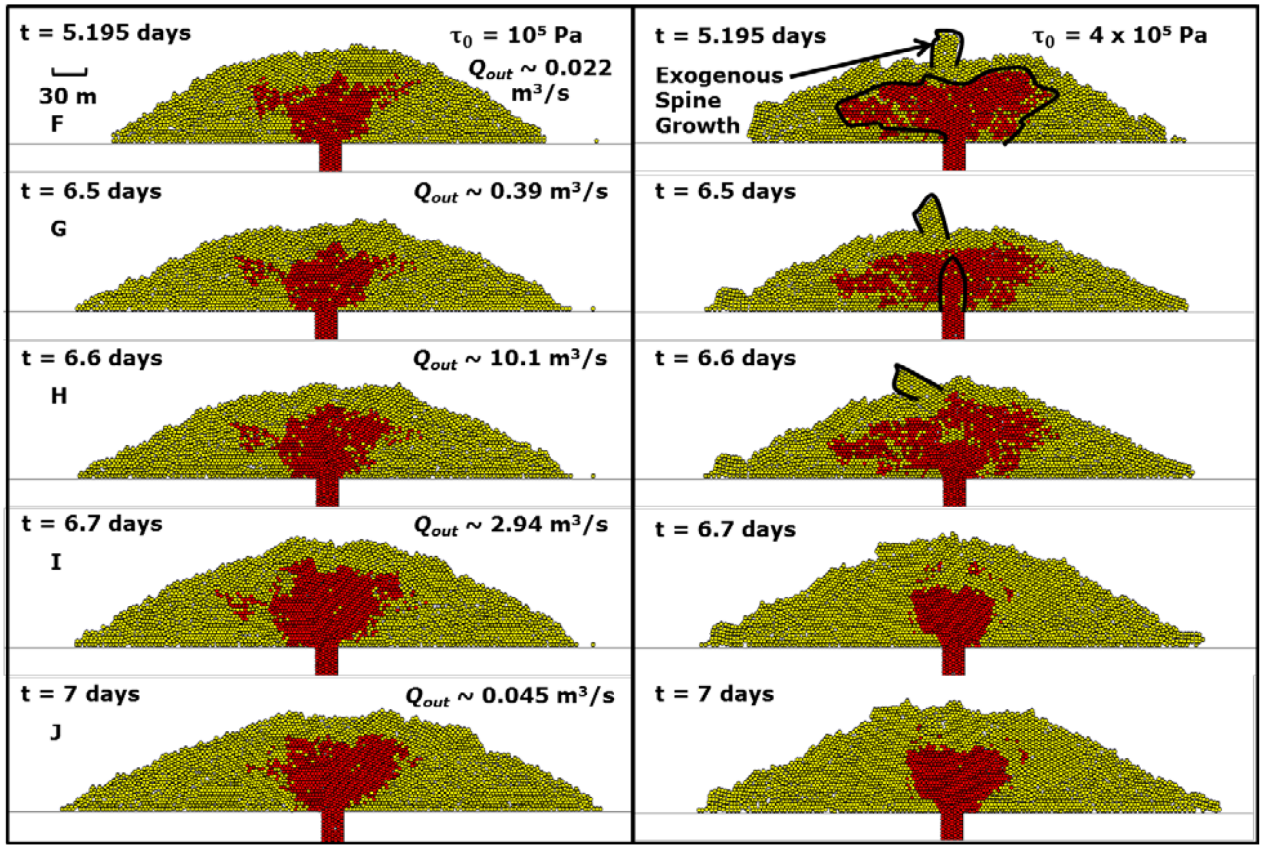

Figure 13. Snapshots of the simulated lava dome morphology for the flow rate history given in Fig. 8. The time intervals at which the snapshots were taken correspond with the labels in Fig. 11 which provide the magnitude of the extruding magma yield strength due to change in crystal content with the periodic flow rate history given in Fig. 9. The simulations are performed for magma with different interparticulate yield strength (τ_0 = 0.1 and 0.4 MPa) with the corresponding snapshots represented above taken at 5.195, 6.5, 6.6, 6.7 and 7 d during the eruption cycle.

transition in growth style from endogenous with ductile core, to shear lobe generation with higher crystal content and yield strength. Endogenous dome growth is observed in the simulation runs for higher flow rates ($Q_{\text{out}} > 2$ m^3 s^{-1}) for both values of τ_0, whereas exogenous spine extrusion occurs at low flow rates ($Q_{\text{out}} < 1$ m^3 s^{-1}) for $\tau_0 > 0.3$ MPa.

5 CONCLUSIONS

We have developed a 2-D particle-mechanics model coupled to equations representing transient conduit flow dynamics. The model accounts for degassing-induced crystallization and variation in crystal content (ϕ) of ascending magma, which influences the magma rheology. The model provides an understanding of the underlying effect of periodic eruptive activity on the evolving morphology of a synthetic lava dome. Dome growth styles are observed to be sensitive to magma yield strength, which is a function of the interparticulate resistance and crystal content of the magma (ϕ), where ϕ is controlled by the magma ascent rate. The transition in magma flow patterns is governed by the interplay of flow rate and magma yield strength, which in turn govern the morphology and spatially varying material properties of the resulting composite lava dome.

Degassing-induced crystallization is promoted at low flow rates, which leads to the development of degassed lava plugs and shear lobes. Our results demonstrate the effect of magma yield strength and varying flow rates on magma rheology. Intermittent spine generation is observed during the evolution of a synthetic lava dome with the properties representing SHV for $Q_{\text{out}} < 2$ m^3 s^{-1} and $\tau_0 > 0.2$ MPa, as shown in Figs 5 and 7. Endogenous shear lobes are developed at higher flow rates (6 m^3 s^{-1} > $Q_{\text{out}} > 2$ m^3 s^{-1}), where the magma crystal content (ϕ) is relatively lower, as shown in Figs 5 and 7 for magma with $\tau_0 = 0.25$ and 0.6 MPa respectively. Evolution of a synthetic lava dome with a ductile core occurs over a range of flow rates ($Q_{\text{out}} = 2$ to 8 m^3 s^{-1}) that depend on the yield strength of the magma. The lava dome grows endogenously with a soft core for the entire range of flow rates ($Q_{\text{out}} = 0.5$ to 8 m^3 s^{-1}) for $\tau_0 = 0.1$ MPa and a ductile core is observed to evolve at $Q_{\text{out}} \geq 2$ m^3 s^{-1} for $\tau_0 \geq 0.25$ MPa.

Our results are able to reproduce periodicity of eruptive activity, and to define its effect on the morphologic evolution of the dome structure. The style of periodicity in our models successfully match the general style of periodicity observed at MSH (see e.g. Barmin *et al.* 2002, Fig. 5a; Swanson & Holcomb 1990). However the lengths of period observed in our models are shorter than at MSH, due to our need to adjust parameters to shorten the calculation run times. The model is capable of reproducing generic sequences showing repeated pulsation with associated rheological changes. We show that the magma chamber volume, interparticulate resistance and ratio of magma viscosity (μ_2/μ_1) significantly affect the evolving structure of the lava dome. Magma is simulated to erupt in pulses, as observed in the periodic dome growth activity at SHV and MSH. The erupted magma experiences cycles of rheological stiffening due to degassing-induced crystallization during the reduced flow rates between distinct pulses of high extrusive

activity (Fig. 8). For a smaller magma chamber with larger value of X_1 (smaller μ_2/μ_1 ratio) a shear lobe develops endogenously for an erupting magma with lower value of τ_0 (>0.4 MPa). The extent of the growth is defined by the duration between successive pulses (time between Points Y_1 and Y_2 in Fig. 8). Spine growth is observed for larger magma chambers with lower values of X_1 (<1 m^3 s^{-1}) and magma with greater values of τ_0 (>0.4 MPa) where the time difference between points Y_1 and Y_2 (Fig. 8) is longer. It is observed that pressure builds up in the magma chamber at lower flow rates (Q_{out}), with these low flow rates causing rheological stiffening of the extruding magma. The result is the development of a viscous plug in the upper conduit that is pushed out by a new pulse of fresh magma.

An important result is that our simulated domes tend to sag and spread following extrusion pulses, with the process actually initiating during the extrusion. The process, which reflects a viscous dome core with retardation by yield strength and talus friction, can be detected visually as reduced dome heights and broadened diameters, represented by dome h/d aspect ratios that reduce with time. For example such changes are shown for post-pulse 2 snapshots D and E (h/d ratios 0.22 → 0.20 and 0.26 → 0.23, respectively for low-strength and high-strength cases). For post-pulse 3, snapshots F and G (h/d 0.23 → 0.18 for the low-strength case, while 0.27 → 0.24 (with spine) and 0.21 → 0.18 (discounting spine) for the high-strength case). Field observations at MSH and elsewhere document the occurrence of such phenomena (Moore *et al.* 1981; Voight *et al.* 2000).

ACKNOWLEDGEMENTS

This work is a partial result of support from NASA under grant NASA-NNX11AC03G. This support is gratefully acknowledged. The work would not have happened without additional research support given to BV, GM and DE by the NSF and UAVCO in the USA and in the UK. BV also appreciates support from the US Geological Survey for his work at Mount St. Helens, and the British Geological Survey and UK Foreign and Commonwealth Office for work on Montserrat. Thoughtful reviews by Oleg Melnik and Benoît Taisne contributed to the final manuscript.

REFERENCES

Anderson, K. & Segall, P., 2011. Physics-based models of ground deformation and extrusion rate at effusively erupting volcanoes, *J. geophys. Res.,* **116**(B7), B07204.

Anderson, S.W. & Fink, J.H., 1990. The development and distribution of surface textures at the Mount St. Helens dome, in *Lava Flows and Domes SE - 2*, pp. 25—46, ed. Fink, J., Springer.

Barmin, A., Melnik, O. & Sparks, R.S.J., 2002. Periodic behavior in lava dome eruptions, *Earth planet. Sci. Lett.,* **199**(1–2), 173–184.

Blake, S., 1990. Viscoplastic models of lava domes, in *Lava Flows and Domes SE - 5*, pp. 88–126, ed. Fink, J., Springer.

Buisson, C. & Merle, O., 2002. Experiments on internal strain in lava dome cross sections, *Bull. Volcanol.,* **64**(6), 363–371.

Cashman, K.V. & Taggart, J.E., 1983. Petrologic Monitoring of 1981 and 1982 Eruptive Products from Mount St. Helens, *Science,* **221**(4618), 1385–1387.

Cashman, K. & Blundy, J., 2000. Degassing and crystallization of ascending andesite and dacite, *Phil. Trans. R. Soc. A,* **358**(1770), 1487–1513.

Cashman, K.V., Thornber, C.R. & Pallister, J.S., 2008. From dome to dust: shallow crystallization and fragmentation of conduit magma during the 2004–2006 Dome Extrusion of Mount St. Helens, Washington, in *A Volcano Rekindled: The Renewed Eruption of Mount St. Helens, 2004–2006*, pp. 387–413, eds Sherrod, D.R., Scott, W.E. & Stauffer, P.H., U. S. Geological Survey.

Costa, A., 2005. Viscosity of high crystal content melts: dependence on solid fraction, *Geophys. Res. Lett.,* **32**(22), L22308, doi:10.1029/2005GL024303.

Costa, A., Melnik, O. & Sparks, R.S.J., 2007. Controls of conduit geometry and wallrock elasticity on lava dome eruptions, *Earth planet. Sci. Lett.,* **260**(1–2), 137–151.

Couch, S., Harford, C.L., Sparks, R.S.J. & Carroll, M.R., 2003. Experimental constraints on the conditions of formation of highly calcic plagioclase microlites at the Soufrire Hills Volcano, Montserrat, *J. Petrol.,* **44**(8), 1455–1475.

Cundall, P.A. & Strack, O.D.L., 1979. A discrete numerical model for granular assemblies, *Géotechnique,* **29**(1), 47–65.

Denlinger, R.P. & Hoblitt, R.P., 1999. Cyclic eruptive behavior of silicic volcanoes, *Geology,* **27**(5), 459–462.

Elsworth, D., Mattioli, G., Taron, J., Voight, B. & Herd, R., 2008. Implications of magma transfer between multiple reservoirs on eruption cycling, *Science,* **322**(5899), 246–248.

Foroozan, R., Elsworth, D., Voight, B. & Mattioli, G.S., 2010. Dual reservoir structure at Soufrière Hills Volcano inferred from continuous GPS observations and heterogeneous elastic modeling, *Geophys. Res. Lett.,* **37**(19), L00E12, doi:10.1029/2010GL042511.

Griffiths, R.W., 2000. The dynamics of lava flows, *Annu. Rev. Fluid Mech.*, **32**(1), 477–518.

Griffiths, R.W. & Fink, J.H., 1997. Solidifying Bingham extrusions: a model for the growth of silicic lava domes, *J. Fluid Mech.,* **347,** 13–36.

Hale, A.J., 2007. Magma flow instabilities in a volcanic conduit: implications for long-period seismicity, *Phys. Earth planet. Inter.,* **163**(1–4), 163–178.

Hale, A.J., 2008. Lava dome growth and evolution with an independently deformable talus, *Geophys. J. Int.,* **174**(1), 391–417.

Hale, A.J. & Wadge, G., 2008. The transition from endogenous to exogenous growth of lava domes with the development of shear bands, *J. Volcanol. Geotherm. Res.,* **171**(3-4), 237–257.

Hale, A.J., Bourgouin, L. & Mühlhaus, H.B., 2007. Using the level set method to model endogenous lava dome growth, *J. geophys. Res.,* **112**(B3), B03213, doi:10.1029/2006JB004445.

Hammer, J.E. & Rutherford, M.J., 2002. An experimental study of the kinetics of decompression-induced crystallization in silicic melt, *J. geophys. Res.,* **107**(B1), ECV 8-1–ECV 8-24.

Hess, K.U. & Dingwell, D.B., 1996. Viscosities of hydrous leucogranitic melts: a non-Arrhenian model, *Am. Mineral.,* **81**(9–10), ECV 8–1-ECV 8–24.

Hort, M., 1998. Abrupt change in magma liquidus temperature because of volatile loss or magma mixing: effects on nucleation, crystal growth and thermal history of the magma, *J. Petrol.,* **39**(5), 1063–1076.

Huppert, H.E. & Woods, A.W., 2002. The role of volatiles in magma chamber dynamics, *Nature,* **420**(6915), 493–495.

Huppert, H.E., Shepherd, J.B., Sigurdsson, H., Stephen, R. & Sparks, J., 1982. On lava dome growth, with application to the 1979 lava extrusion of the soufrière of St. Vincent, *J. Volcanol. Geotherm. Res.,* **14**(3–4), 199–222.

Husain, T., Elsworth, D., Voight, B., Mattioli, G. & Jansma, P., 2014. Influence of extrusion rate and magma rheology on the growth of lava domes: insights from particle-dynamics modeling, *J. Volcanol. Geotherm. Res.,* **285,** 100–117.

Jaupart, C. & Tait, S., 1990. Dynamics of eruptive phenomena, *Rev. Mineral. Geochem.,* **24**(1), 213–238.

Lavallée, Y., Hess, K.-U., Cordonnier, B. & Dingwell, D.B., 2007. Non-Newtonian rheological law for highly crystalline dome lavas, *Geology,* **35**(9), 843–846.

Lejeune, A.-M. & Richet, P., 1995. Rheology of crystal-bearing silicate melts: An experimental study at high viscosities, *J. geophys. Res.,* **100**(B3), 4215–4229.

Lipman, P.W., Norton, D.R., Taggart, J.E., Brandt, E.L. & Engleman, E.E., 1981. Compositional variation in 1980 magmatic deposits, in *The 1980 Eruption of Mount St. Helens, Washington,* 1250th edn, pp. 631–640, United States Geological Survey Professional Paper.

Lyman, A.W., Kerr, R.C. & Griffiths, R.W., 2005. Effects of internal rheology and surface cooling on the emplacement of lava flows, *J. geophys. Res.,* **110**(B8), B08207, doi:10.1029/2005JB003643.

Marsh, B.D., 1981. On the crystallinity, probability of occurrence, and rheology of lava and magma, *Contributions to Mineralogy and Petrology,* **78**(1), 85–98.

Marsh, B.D., 1998. On the interpretation of crystal size distributions in magmatic systems, *J. Petrol.,* **39**(4), 553–599.

Mastin, L.G., 2002. Insights into volcanic conduit flow from an open-source numerical model, *Geochem. Geophys. Geosyst.,* **3**(7), 1–18.

Mastin, L.G., Roeloffs, E., Beeler, N.M. & Quick, J.E., 2008. Constraints on the size, overpressure, and volatile content of the Mount St. Helens magma system from geodetic and dome-growth measurements during the 2004–2006 Eruption, in *A Volcano Rekindled: The Renewed Eruption of Mount St. Helens, 2004–2006*, pp. 461–488, eds Sherrod, D.R., Sherrod, W.E. & Sherrod, P.H., U. S. Geological Survey.

Melnik, O. & Sparks, R.S.J., 1999. Nonlinear dynamics of lava dome extrusion, *Nature,* **402**(6757), 37–41.

Melnik, O. & Sparks, R.S.J., 2002. Dynamics of magma ascent and lava extrusion at Soufrière Hills Volcano, Montserrat, *Geol. Soc. London Mem.,* **21**(1), 153–171.

Melnik, O. & Sparks, R.S.J., 2005. Controls on conduit magma flow dynamics during lava dome building eruptions, *J. geophys. Res.,* **110**(B2), B02209, doi:10.1029/2004JB003183.

Moore, J.G., Lipman, P.W., Swanson, D.A. & Alpha, T.R., 1981. Growth of lava domes in the crater, June 1980–January 1981, in *The 1980 Eruptions of Mount St. Helens, Washington,* 1250th edn, pp. 541–547, United States Geological Survey Professional Paper.

Morgan, J.K. & McGovern, P.J., 2005a. Discrete element simulations of gravitational volcanic deformation: 1. Deformation structures and geometries, *J. geophys. Res.,* **110**(B5), B05402, doi:10.1029/2004JB003252.

Morgan, J.K. & McGovern, P.J., 2005b. Discrete element simulations of gravitational volcanic deformation: 2. Mechanical analysis, *J. geophys. Res.,* **110**(B5), B05403, doi:10.1029/2004JB003253.

Murase, T., McBirney, A.R. & Melson, W.G., 1985. Viscosity of the dome of mount St. Helens, *J. Volcanol. Geotherm. Res.,* **24**(1–2), 193–204.

Odbert, H.M., Stewart, R.C. & Wadge, G., 2014. Chapter 2 Cyclic phenomena at the Soufrière Hills Volcano, Montserrat, *Geol. Soc. London Mem.,* **39**(1), 41–60.

Pallister, J., Hoblitt, R.P., Crandell, D.R. & Mullineaux, D.R., 1992. Mount St. Helens a decade after the 1980 eruptions: magmatic models, chemical cycles, and a revised hazards assessment, *Bull Volcanol*., **54**(2), 126–146.

Pinkerton, H. & Stevenson, R.J., 1992. Methods of determining the rheological properties of magmas at sub-liquidus temperatures, *J. Volcanol. Geotherm. Res.,* **53**(1–4), 47–66.

Rutherford, M.J. & Hill, P.M., 1993. Magma ascent rates from amphibole breakdown: an experimental study applied to the 1980-1986 Mount St. Helens eruptions, *J. geophys. Res.,* **98**(B11), 19 667–19 685.

Saar, M.O., Manga, M., Cashman, K.V. & Fremouw, S., 2001. Numerical models of the onset of yield strength in crystal–melt suspensions, *Earth planet. Sci. Lett.,* **187**(3–4), 367–379.

Shaw, H.R., 1965. Comments on viscosity, crystal settling, and convection in granitic magmas, *Am. J. Sci.,* **263**(2), 120–152.

Simmons, J., Elsworth, D. & Voight, B., 2005. Classification and idealized limit-equilibrium analyses of dome collapses at Soufrière Hills volcano, Montserrat, during growth of the first lava dome: November 1995–March 1998, *J. Volcanol. Geotherm. Res.,* **139**(3–4), 241–258.

Sparks, R.S.J., 1997. Causes and consequences of pressurisation in lava dome eruptions, *Earth planet. Sci. Lett.,* **150**(3-4), 177–189.

Sparks, R.S.J. *et al.*, 1998. Magma production and growth of the lava dome of the Soufriere Hills Volcano, Montserrat, West Indies: November 1995 to December 1997, *Geophys. Res. Lett.,* **25**(18), 3421–3424.

Sparks, R.S.J., Murphy, M.D., Lejeune, A.M., Watts, R.B., Barclay, J. & Young, S.R., 2000. Control on the emplacement of the andesite lava dome of the Soufriere Hills volcano, Montserrat by degassing-induced crystallization, *Terra Nova,* **12**(1), 14–20.

Stasiuk, M.V. & Jaupart, C., 1997. Lava flow shapes and dimensions as reflections of magma system conditions, *J. Volcanol. Geotherm. Res.,* **78**(1–2), 31–50.

Swanson, D.A. & Holcomb, R.T., 1990. Regularities in growth of the Mount St. Helens dacite dome, 1980–1986, in *Lava Flows and Domes SE - 1*, pp. 3–24, ed. Fink, J., Springer.

Voight, B., Hoblitt, R.P., Clarke, A.B., Lockhart, A.B., Miller, A.D. & Lynch, L., 1998. Remarkable cyclic ground deformation monitored in real-time on Montserrat, and its use in eruption forecasting, *Geophys. Res. Lett.,* **25**(18), 3405–3408.

Voight, B. *et al.*, 1999. Magma Flow instability and cyclic activity at Soufriere Hills Volcano, Montserrat, British West Indies, *Science,* **283**(5405), 1138–1142.

Voight, B. *et al.*, 2000. Deformation and seismic precursors to dome-collapse and fountain-collapse nuées ardentes at Merapi Volcano, Java, Indonesia, 1994–1998, *J. Volcanol. Geotherm. Res.,* **100**(1–4), 261–287.

Wadge, G., Herd, R., Ryan, G., Calder, E.S. & Komorowski, J.-C., 2010. Lava production at Soufrière Hills Volcano, Montserrat: 1995–2009, *Geophys. Res. Lett.,* **37**(19), L00E03, 10.1029/2009GL041466.

Watts, R.B., Herd, R.A., Sparks, R.S.J. & Young, S.R., 2002. Growth patterns and emplacement of the andesitic lava dome at Soufrière Hills Volcano, Montserrat, *J. Volcanol. Geotherm. Res.,* **283**(1), 115–152.

Young, S.R., Voight, B. & Duffell, H.J., 2003. Magma extrusion dynamics revealed by high-frequency gas monitoring at Soufrière Hills volcano, Montserrat, *Geol. Soc. London Spec. Publ.,* **213**(1), 219–230.